SCIENTIFIC REPORT 2001-2003

NEST
National Enterprise for nanoScience and nanoTechnology

NEST, the National Enterprise for nanoScience and nanoTechnology, was established in May 2001 by the Istituto Nazionale per la Fisica della Materia at Scuola Normale Superiore in Pisa following selection of the proposal by an international panel.
NEST was designed to compete with the centers of excellence being established in the most technologically advanced countries in the field of nanoscience and to become a reference point and a resource for the INFM community. As stated in its original proposal, "cultural and scientific advancement are its main targets in an effort to contribute to fulfill INFM mission".

NEST absorbed the Physics Laboratory of Scuola Normale Superiore and is temporarily located in the Laboratory's original home in Via della Faggiola, a historic building adjacent to Piazza dei Cavalieri, the main seat of Scuola Normale Superiore. At present NEST occupies two floors of the building over an extension of about 900 square meters. Additional laboratories are located at the Physics Department of the University of Pisa and at TASC-INFM in Trieste. NEST has largely outgrown its available laboratory and office space. Its new home is currently being built by Scuola Normale Superiore in the San Silvestro complex, a significant financial effort that will adequately house NEST and its ambitious growth goals.

These first two years have seen an extraordinary development from all points of view: new personnel, new scientific lines and, above all, scientific results that have much exceeded the goals stated in the original proposal.

Research was funded through the NEST grant and additional grants from several agencies including the Italian Ministry of Research, the Ministry of Economy, the European Commission, Consiglio Nazionale delle Ricerche, Fondazione Monte dei Paschi, Fondazione Cassa di Risparmio di Pisa, Istituto Nazionale per la Fisica della Materia, Human Frontier Science Program. Significant funding was obtained from collaborative contracts with industrial companies (both from within Europe and from the USA).

Further information on NEST activities, facilities, collaborations and support can be found at www.nest.sns.it.

Fabio Beltram
May 2003

PERSONNEL

DIRECTOR Fabio Beltram

SECRETARIAT Valentina Cascella
Aldo Rizzo

EXECUTIVE COMMITTEE

Fabio Beltram	Rosario Fazio
Mauro Giacca	Vittorio Pellegrini
Lucia Sorba	Mario Tosi

SCIENTIFIC COMMITTEE

Michele Parrinello (INFM representative)
Mario Tosi (Scuola Normale representative)
Allan MacDonald
Michael Pepper
Aron Pinczuk

RESEARCH STAFF

Zehra Akdeniz
Luigi Amico
Fabio Beltram
Giorgio Biasiol
Ranieri Bizzarri
Sergio Caracciolo
Franco Carillo
Anna Cereseto
Alberto Di Lieto
Riccardo Farchioni
Rosario Fazio
Mauro Giacca
Paolo Giannozzi
Gaetano Giaquinta
Francesco Giazotto
Michele Governale
Renzo Grassi
Giuseppe Grosso
Jean-Marc Jancu
Marco Lazzarino
Alessandro Marcello
Anna Minguzzi
G. Massimo Palma
Daniela Parisi
Giuseppe Pastori Parravicini
Vittorio Pellegrini
Vincenzo Piazza
Pasqualantonio Pingue
Marco Polini
Roberto Raimondi
Lucia Sorba
Fabio Taddei
Alessandra Toncelli
Mauro Tonelli
Mario P. Tosi
Valentina Tozzini
Alessandro Tredicucci
Giovanni Vignale
Patrizia Vignolo
Jihua Xu

POST DOCTORAL STAFF

Caterina Arcangeli
Reza Asgari
Pablo Capuzzi
Maria Luisa Chiofalo
Roberto D'Agosta
Bahman Davoudi
Wilfried Desrat
Diego Frustaglia
Armando Gama Goicochea
Andrea Mastellone
Simone Montangero
Andreas Osterloh
Kumar Mukesh
Francesco Plastina
Barbara Ressel
Mudit Tyagi

GRADUATE STUDENTS

Silvia Agostini
Aji Anappara Akhileswaran
Mohamed Alshourbagy
Reza Bakhtiari
Francesco Banfi
Stefano Bigotta
Francesco Capurro
Marco Cecchini
Alessandro Cresti
Francesco Cornacchia
Gabriele De Chiara
Aldo Ferrari
Antonio Fittipaldi
Rüdeger Köhler
Teodoro Laino
Stefano Luin
Riccardo Nifosì
Luigi Palatella
Roberta Paolinelli
Cesar Pascual Garcia
Dania Puggioni
Kalai Kumar Rajagopal
Stefano Roddaro
Alessandro Romito
Arianna Sabò
Elisa Sani
Giuseppe Sica
Janine Splettstoesser
Ennio Tasciotti
Maria Elena Terreni
Michele Virgilio

LAUREA STUDENTS

Luca Alloatti
Pietro Amat
Chiara Bertini
Lucia Bonelli
Michele Brondi
Flavio Capotondi
Francesco Cardarelli
Vincenzo Carnevale
Carlo Castellana
Alessandra Chesi
Giorgio De Simoni
Dimitri Dini
Daniele Ercolani
Yasa Eksioglu
Elena Favilla
Kasper Grove Rasmussen
Carla Linguardo
Lukas Mahler
Cosimo Mauro
Giorgio Mori
Alessia Ravani
Matteo Rizzi
Saverio Russo
Nicola Totò
Francesca Traverso

TECHNICAL STAFF

Pietro Barnini
Paolo Faraci
Ilaria Grassini
Bruno Guidi
Claudio Lelli
Alessandro Masetti
Fabio Torri

EXPERIMENTAL FACILITIES

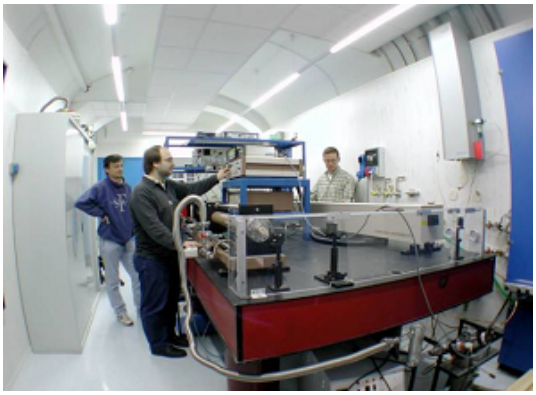


- Magnetotransport and magnetooptical studies (from NIR to UV) down to 10 mK, under magnetic fields up to 16 Tesla;
- Transport and submicron-resolution optical studies down to 1.2 K (from visible to NIR);
- MIR and FIR spectroscopy down to 1.2 K;
- STM (UHV) and AFM (air) studies;
- Nanofabrication in clean-room environment (UV & electron-beam lithography, thermal evaporation, RIE, PECVD, STM and AFM techniques);
- Fabrication of hybrid superconductor-semiconductor junctions by a UHV surface-preparation (RF backsputtering) and characterization systems (STM & RHEED) integrated with a superconductor DC sputtering-deposition chamber;
- Cell culture and manipulation;
- High-sensitivity (spectral and spatial) studies on living cells;
- Single-molecule imaging;
- Protein spectroscopy and chromatography.

NEST is equipped with machine and electronic shops and its own computing facilities.


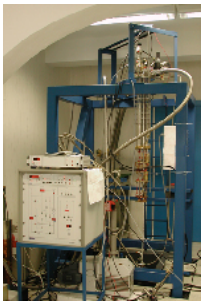


SCIENTIFIC ACTIVITY

According to the programme, NEST is organized in four Research Activities (RAs):

- Coherent nanoelectronics
- Nanobiotechnology
- Spin electronics
- Theory of electron liquids in nanostructures

all four were implemented along the lines of the original proposal. Their productivity is shown by the publication list that concludes this report. Fourteen research lines and their main published results were selected from all RAs and are presented in greater detail in the following.

Here we should like to highlight some of the most significant results obtained in research areas of particular and timely relevance. These include the realization of THz heterostructure lasers that find a large variety of applications ranging from pollution monitoring to medical diagnostics [R. Koehler et al. Nature (2002) and subsequent publications], proposals for novel schemes and concepts for quantum communication and cryptography [R. Fazio et al. Nature (2002)], demonstration of optical storage based on single biomolecules [R. Cinelli et al. Appl. Phys. Lett. (2001)], identification of novel protein-protein interactions involved in HIV-1 replication by fluorescence resonant energy transfer [A. Marcello et al. EMBO J. (2003)], observation of soft collective modes and spin phases in low-dimensional electron systems by resonant inelastic light scattering [S. Luin et al. Phys. Rev. Lett. (2003)], and demonstration of non-linear transport of quasiparticles in fractional quantum Hall mesoscopic systems [S. Roddaro et al. Phys. Rev. Lett. (2003)]. The resonance of these publications in the media contributed much to the visibility of the Center among the general public.

In the following, **14 selected research lines** will be presented:

TERAHERTZ SEMICONDUCTOR-HETEROSTRUCTURE LASERS

Rüdeger Köhler, Alessandro Tredicucci, Cosimo Mauro, Fabio Beltram

A substantial and growing part of modern technology is using semiconductor devices for the generation of electromagnetic radiation. Visible and infra-red (IR) diode lasers are at the core of new systems of information exchange, storage and retrieval. Equally, microwave and radio-frequency emitters are enabling the widespread exploitation of wireless communications with an ever increasing degree of sophistication. The terahertz region of the spectrum, on the other hand, has remained largely untouched by this rapid stream of innovation, so much that is was nicknamed the 'THz gap'. In fact, electronics typically fails at such high frequencies whilst laser diodes based on narrow-gap materials face several fundamental and technological limitations when extended to such long emission wavelengths. Consequently the region in the electromagnetic spectrum spanning approximately from 1 to 10 THz lacks the availability of compact solid-state emitters. This is in sharp contrast with the demand for practical sources in fields like medical imaging, security controls, remote sensing and high-bandwidth wireless communication. The peculiar transparency of various substances in this spectral region makes it a perfect choice for the study of biological tissues, for revealing concealed items, and for implementing intra-building communication links [1]. Here, we describe the development of a THz semiconductor heterostructure laser which possesses the potential for device-like implementations and thus represents a first step towards the development of widely usable THz photonics.

Conventional semiconductor lasers generate light via the recombination of conduction-band electrons with valence-band holes. In contrast, in quantum cascade (QC) lasers electrons travel through a potential staircase of coupled quantum wells where the conduction band is split by quantum confinement into a number of distinct subbands. The electron wavefunctions and energies can be controlled by layer thickness and applied bias, which allow tailoring of electronic and optical properties. Population inversion between two subbands is then achieved by engineering tunneling and scattering times. To this end, the active regions, which host the two lasing subbands, are interlaced with injector sections extracting electrons from the previous active region, cooling down the electron population and finally injecting the carriers again into the upper laser level of the following active region. QC lasers were first demonstrated at mid-infrared wavelengths [2], but were immediately recognized as a promising candidate for a device-like THz semiconductor laser. However, despite a notable extension of the emission wavelength and tremendous improvements in their performance [3], only electroluminescence could be observed at THz frequencies [4]. Significant issues to be addressed included the challenge of achieving population inversion at such small energies and the creation of a waveguide providing sizeable optical confinement to the epilayer structure. In mid-IR QC lasers, population inversion can be conveniently achieved by controlling the emission of longitudinal optical

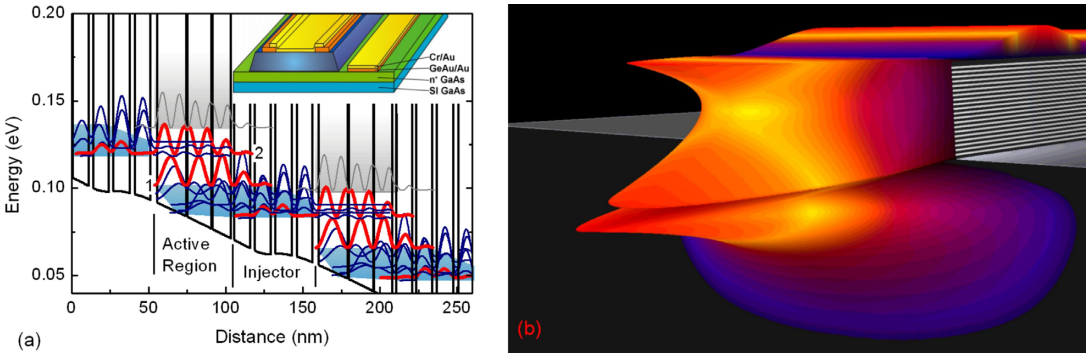

Figure 1 (a) Self-consistent calculation of a portion of the conduction band structure in the active core of the laser. Shown are the moduli squared of the relevant wavefunctions, the optical transition being between the two states (2 and 1) drawn in red. The minibands are represented by the shaded areas. Electrons are injected into the upper laser level 2 via resonant tunneling from the ground state of the injector miniband. Inset: schematic view of a processed laser bar. **(b)** Three-dimensional, illustrative representation of the optical mode traveling along the waveguide. The cut into the mode at the bottom of the ridge is caused by the bottom contact layer. The mode intensity is depicted in a color-scale ranging from blue to red.

phonons by the electrons in the two optically active subbands. However, the situation becomes more complicated for photon energies in the THz region, i.e. below the phonon reststrahlenband, where other processes like carrier-carrier scattering play a relevant role. In our laser, the optical transition takes place between the first and second miniband of a specifically engineered chirped superlattice. Figure 1(a) shows a self-consistent calculation of a portion of the conduction band structure with the two laser states drawn in red. They are delocalized across several quantum wells leading to a large dipole matrix element for the optical transition. Our design aims at minimizing the population of the lower laser level 1 while still maintaining a sufficiently long lifetime of level 2. To this end, 1 is strongly coupled to a wide and dense injector miniband. This leads to fast extraction of carriers and reduces re-population of the lower laser level by providing a large phase space for electrons to spread. Also, the large dispersion of the miniband allows for a large operating range of voltages and currents and hinders thermal backfilling from the injector. These considerations were confirmed by simulations of the electronic transport, which predicted a population inversion of 1.1×10^9 cm^{-2} leading to an optical gain of 31 cm^{-1} [5,6]. Carrier distribution was calculated by sampling a coupled set of fully three-dimensional Boltzmann equations via a Monte-Carlo technique. Electron dynamics was computed taking into account both carrier-carrier and carrier-phonon scattering processes, and, thanks to periodic boundary conditions, the full voltage-current characteristics was obtained [7].

The second issue is related to the laser resonator: conventional waveguides are inappropriate owing to the large optical losses due to free-carrier absorption and practical limitations in epilayer growth resulting in a poor overlap of the optical mode with the active medium. An almost unity confinement factor of the radiation over an active medium of any thickness can be achieved by sandwiching the semiconductor between two metals. This is, however, realized at the expense of high propagation losses resulting from the residual penetration of the mode into the metal claddings. In our waveguide instead the mode is guided by a thin high-doped GaAs layer inserted directly underneath the active core of the laser. The high doping concentration in this layer renders its dielectric constant negative and thus of opposite sign compared to that of the surrounding material. In such a configuration, Maxwell's equations give rise to peculiar solutions, called surface plasmons, that propagate along each interface decaying exponentially away from them. In the present case, owing to the long wavelength of the light compared to the penetration depth into the guiding layer, the two surface plasmons at the two interfaces actually merge into a single mode. We then tailored doping concentration and thickness of the layer to achieve a high overlap of the mode with the active core, at the same minimizing absorption losses [5]. This highly doped layer is simultaneously used as bottom contact and the waveguide is completed by a top metallic contact. A schematic view of the resulting mode profile in a processed laser is shown in Fig. 1 (b).

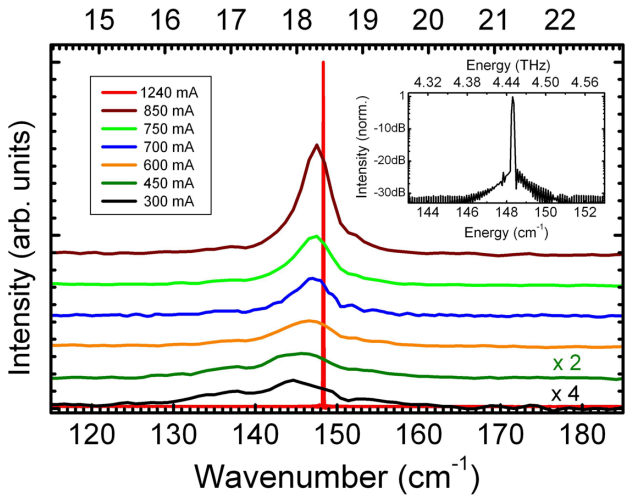

Figure 2 Emission spectra from a 1.24 mm long and 180 µm wide laser ridge recorded at different drive currents. The laser spectrum is scaled down by several orders of magnitude. With increasing current, the characteristic narrowing and non-linear intensity dependence of the emission line is observed. Passing laser threshold at 880 mA, single-mode emission is observed at 4.4 THz with a side-mode suppression ratio better than 20 dB (see inset).

Samples were grown by molecular beam epitaxy onto semi-insulating GaAs substrates and wafers were processed by optical lithography and wet chemical etching into ridge-geometry stripes. Electrical contacts were formed to selected areas on the top of the ridges and on the bottom contact layer (see inset of Fig. 1(a)). Fabry-Perot cavities were obtained by cleaving and the facets were either left untreated or a high-reflection coating was deposited onto the back facet. (see Ref. [5,8] for details). Lasers were mounted onto the cold finger of a continuous-flow He-cryostat

and spectral measurements were taken with a Fourier-transform infrared spectrometer (FTIR) [5]. Figure 2 shows the spectra recorded from such a device as function of drive current. The characteristic narrowing of the emission line with increasing current is clearly visible up to about 880 mA, where laser threshold is reached. A single lasing mode at 4.4 THz is obtained, as shown in the inset where the logarithmic scale highlights the side-mode suppression ratio by more than 20 dB.
The first devices could be operated in pulsed mode up to 50 K with output powers of about 2.5 mW and duty cycles up to 20 %. Since then, we optimized processing and fabrication to reduce waveguide losses and Joule heating. Further improvement in laser performance is attained when a high-reflection coating is deposited onto the back facet of the laser. This improved fabrication allowed an increase in the maximum operating temperature to 75 K, with collected peak output powers of about 5 mW. Continuous wave operation was also obtained with similar power performance up to a maximum temperature of about 50 K. At the same time new developments in the quantum design of the active region resulted in the realization of lasers at the even lower frequencies of 3.5 THz [9] (and very recently 2.8 THz) with similar performance and threshold current densities as low as 100 A/cm^2. Beyond the extension to frequencies 1-3 THz, which are the most interesting for many applications, the other fundamental research target for the advancement of THz QC laser technology is the study of structure and device concepts that could allow operation at higher temperatures. A first step in this direction is represented by so-called interdigitated structures, in which phonon relaxation stages are alternated with the optically active regions. Figure 3 shows the pulsed L-I characteristics of one such interdigitated laser. Clearly the temperature performance is much improved, although the threshold current density is not particularly low, probably due to non-perfect injection efficiency. A maximum operating temperature of 94 K is recorded with high output powers of more than 6 mW at 30 K and about 2 mW at 80 K (the power, as in the previous cases, is recorded with a pyroelectric radiometer, providing an estimated collection efficiency of 33%).

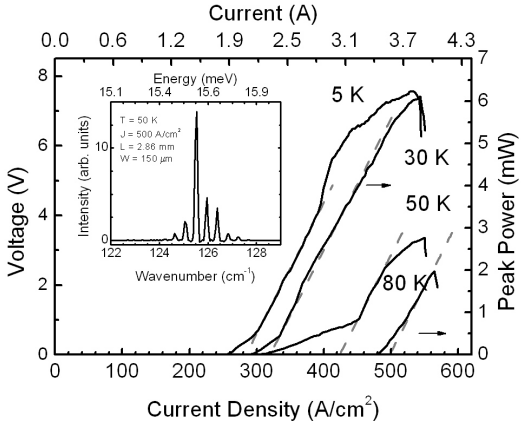

Figure 3 Collected peak output power as a function of drive current from an interdigitated laser 150 µm wide and 4.7 mm long at various heat-sink temperatures. In the inset a typical Fabry-Perot emission spectrum as recorded from a shorter laser stripe at 50 K is reported.

Collaborations

This activity is carried out in collaboration with the Cavendish Laboratory of Cambridge University and INFM-Politecnico di Torino.

References

[1] D. Mittleman (Ed.): *Sensing with Terahertz Radiation* (Springer, Berlin, 2002).
[2] J. Faist, F. Capasso, D. L. Sivco, C. Sirtori, A. L. Hutchinson, and A. Y. Cho, Science **264**, 553 (1994).
[3] M. Beck, D. Hofstetter, T. Aellen, J. Faist, U. Oesterle, M. Illegems, E. Gini, and H. Melchior, Science **295**, 301 (2002).
[4] See, for instance, R. Köhler, A. Tredicucci, F. Beltram, H. E. Beere, E. H. Linfield, A. G. Davies, and D. A. Ritchie, Appl. Phys. Lett. **80**, 1867 (2002), and references therein.
[5] R. Köhler, A. Tredicucci, F. Beltram, H. E. Beere, E. H. Linfield, A. G. Davies, D. A. Ritchie, R. C. Iotti, and F. Rossi, Nature **417**, 156 (2002).
[6] R. Köhler, R. C. Iotti, A. Tredicucci, and F. Rossi, Appl. Phys. Lett. **79**, 3920 (2001).
[7] R. C. Iotti and F. Rossi, Phys. Rev. Lett. **87**, 146603-I (2001).
[8] R. Köhler, A. Tredicucci, F. Beltram, H. E. Beere, E. H. Linfield, A. G. Davies, D. A. Ritchie, S. Dhillon, and C. Sirtori, Appl. Phys. Lett. **82**, 1518 (2003).
[9] R. Köhler, A. Tredicucci, F. Beltram, H. E. Beere, E. H. Linfield, A. G. Davies, and D. A. Ritchie, Opt. Lett. **28**, 810 (2003).

INTERSUBBAND CAVITY ELECTRODYNAMICS

Dimitri Dini, Rüdeger Köhler, Alessandro Tredicucci, Giorgio Biasiol, Lucia Sorba

The interaction of light with material excitations can be completely altered in microcavity structures where the electromagnetic field is confined and the photonic density of states deeply modified. In particular, if the coupling between the optical transition and the radiation is sufficiently strong compared to the damping rates, new elementary excitations, eigenstates of the full photon-matter Hamiltonian, take form and are usually named "cavity polaritons". They present a characteristic anti-crossing behavior, with a mode separation often referred to as "vacuum-field Rabi splitting", in analogy to the well-known Rabi splitting of saturable two-level systems. The study of these phenomena started some time ago in atomic physics [1] and is still attracting a lot of interest especially in connection with research on quantum computation [2]. In the semiconductor world, cavity electrodynamics has developed mainly in conjunction with excitonic states in a variety of systems, from quantum wells (QWs) [3] to bulk [4], from III-V compounds to II-VI. It is currently a very active field, thanks mostly to the latest advances concerning polariton parametric amplification [5] and exciton condensation [6].

Intersubband transitions between confined electronic levels within the conduction band of a semiconductor heterostructure are becoming more and more relevant in understanding the physics of collective excitations of the two-dimensional electron gas (2DEG), and are finding successful application in a number of photonic devices, like QW infrared photodetectors and quantum cascade lasers. Their interaction with cavity photons in micro-resonators, however, is still a largely unexplored subject. There are in fact various practical difficulties which tend to complicate the implementation of monolithic intersubband microcavities. The TM polarization selection rule, for instance, requires unusual geometries to achieve a high quality factor with effective light coupling, while the typical mid-infrared wavelength results in rather large semiconductor layer thickness. Yet the potential appeal is quite high, thanks to the possibility of externally controlling charge density and transition matrix elements and to the fast relaxation times. Moreover, intersubband transitions enjoy a close similarity to atomic ones, as a consequence of their ideally delta-like joint density of states and of the huge separation from continuum levels. Recent theoretical calculations have predicted that intersubband cavity polaritons can indeed be observed in planar resonators for oblique incidence by exploiting total internal reflection at the air interface [7].

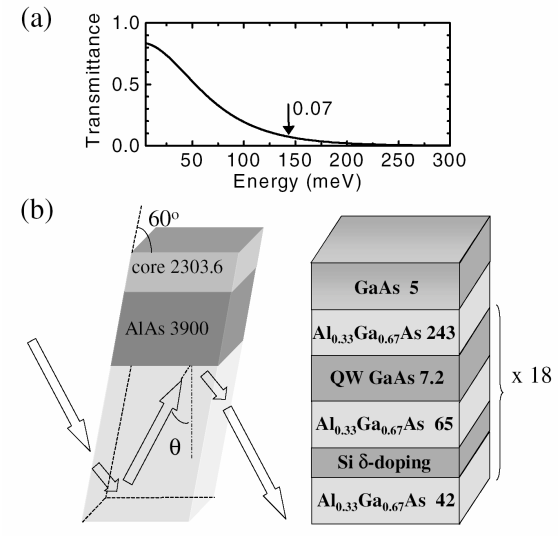

Figure 1 (a) Calculated transmittance of a 3.9 μm thick layer of AlAs embedded in GaAs at an angle of incidence of 60°; the arrow indicates the energy of the chosen intersubband transition (143 meV). **(b)** Schematic view of the prism-shaped micro-resonator. The right panel shows the structure of the active core; thickness values are given in nm.

Here we show the experimental observation of the vacuum-field Rabi splitting of an intersubband transition inside a planar microcavity with multiple 2DEGs embedded [8]. The dispersion of the resulting intersubband polaritons was measured through angle-resolved reflectance measurements using a prism-like geometry, and anti-crossing energies of more than 10 meV were observed up to room temperature. The resonator implemented in this study is fully based on total internal reflection. In fact, distributed Bragg reflectors (DBRs) present at large incidence angles a much smaller reflectance value for TM polarization, and would then have to be impractically thick. In our structure the radiation is instead confined between the semiconductor-air interface on one side (sample surface) and a low refractive index AlAs layer on the other. Above the critical angle this AlAs layer effectively acts as a low-pass filter for the light, as exemplified in Fig. 1(a): at 60° in a GaAs matrix a few micron thickness is

enough to achieve reflectance values of more than 90% for wavelengths shorter than 10 μm. The experimental geometry can then simply make use of the sample substrate, appropriately shaped in a wedge-prism configuration, to obtain the required incidence angle at the cavity surface, as shown in Fig. 1(b). The whole structure was grown by solid-source MBE on an undoped GaAs (001) substrate. It consists of a 3.9 μm thick layer of AlAs followed by eighteen 7.2 nm wide GaAs QWs separated by 107 nm thick $Al_{0.33}Ga_{0.67}As$ barriers; the latter are Si δ-doped ($n_{Si} = 6 \times 10^{11}$ cm^{-2}) with 65 nm- and 42 nm-thick spacers below and above the wells, respectively. The well width was chosen in order to have the transition between the first and second subbands at about 9 μm wavelength, as short as possible but sufficiently far from the continuum and in a spectral region relatively free from atmospheric absorption. The last $Al_{0.33}Ga_{0.67}As$ barrier has a thickness of 243 nm to give the correct cavity length for 60° angle propagation. The latter was designed to be λ/2 of the transition; note however that the wave dephasing at both total internal reflections is different from π (particularly at the interface with the AlAs layer), which must be compensated in the cavity thickness. We checked the uniformity of the carrier density among the 18 QWs by measuring the Shubnikov-de Haas (SdH) oscillations on Van der Pauw structures at 1.5K and magnetic fields up to 5 T. A single oscillation frequency was recorded, corresponding to a carrier sheet density of 4.17×10^{11} cm^{-2}. For the reflectance measurements the resonator was mechanically lapped into wedge-shaped prisms, with the facets at an angle of 60° with respect to the cavity plane (see Fig. 1).

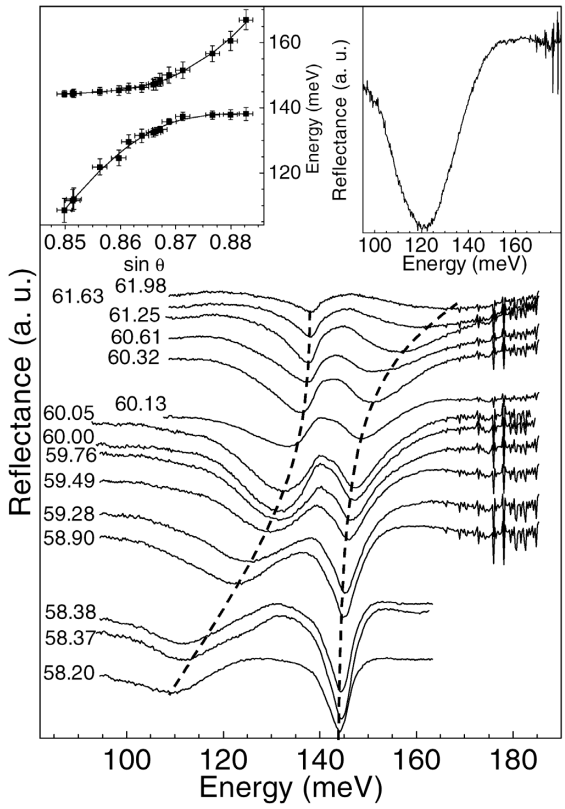

Figure 2 Reflectance of the microcavity sample for different angles of incidence in TM polarization. The spectra were collected at 10 K, with a resolution of 2 cm^{-1}. The angle values refer to θ at the substrate-cavity interface; dashed lines are just a guide to the eye. The spectra are offset from each other for clarity. The rapid oscillations in the high energy portion are due to residual water vapor absorption in the FTIR system. In the left inset the experimental points corresponding to the energy position of the dips are reported. The solid lines are fitted with a standard dipole oscillator dispersion. The right inset contains a spectrum recorded under TE polarization.

Figure 2 shows TM reflectance spectra in the frequency range of the intersubband transition measured at 10 K for different incidence angles. Two dips can be clearly identified, with a typical anti-crossing behavior. By increasing the angle, the cavity mode is tuned across the intersubband one, until at resonance they mix and become strongly coupled, giving rise to intersubband polaritons with a splitting of around 14 meV. The resonance energy of the intersubband transition is about 142 meV, in very good agreement with the 143 meV computed with self-consistent calculations including dynamical many-body contributions like excitonic and depolarization shifts. Its linewidth was measured using a 45° wedged prism to exclude any possible cavity effect and a full-width-at-half-maximum (FWHM) of 5 meV was recorded. This very low value demonstrates the high quality and good uniformity of the quantum wells. On the other hand, the cavity mode has a FWHM of almost 15 meV. This value is larger than expected (a few meV) and is probably due to the non-ideal reflectance of the cavity surfaces (roughness, etc.) and to the angle spread of the incident light beam. It is anyway worth pointing out that, at perfect anti-crossing, the two fully mixed modes tend to share a nearly common linewidth, average of the two individual ones. For comparison, in the right inset of Fig. 2 we report a TE reflectance spectrum. Only the single

cavity mode is visible, as in this polarization the intersubband transition is dipole-forbidden, owing to the well-known selection rule. In the left inset the energy position of the dips is plotted as a function of angle, to evidence the polariton anti-crossing behavior. The dispersion appears to agree quite well with that of a simple Lorentzian dipole oscillator. The polaritonic dispersion of the intersubband-cavity modes remains clearly visible up to room temperature. As in the case of cryogenic temperatures, the anti-crossing presents a well defined polariton splitting of approximately 11 meV. This value is slightly lower than at 10 K, probably a consequence of charge redistribution between the subbands.

In order to obtain a more quantitative description of the experimental data, we have performed a calculation of the structure reflectance using the transfer-matrix formalism. The contribution of the intersubband transition within the 2DEGs has been considered by including in the dielectric permittivity ε of the quantum well layers an additional term in the form of a collection of classical polarized Lorentz oscillators:

$$\varepsilon = \varepsilon_\infty + \frac{N_s e^2 f \sin^2 \vartheta}{m_0 \varepsilon_0 L_{eff}} \frac{1}{\omega_0^2 - \omega^2 - i\Gamma\omega},$$

in which ε_∞ is the quantum well high-frequency dielectric constant, N_s is the electronic sheet density, e the electronic charge, f the oscillator strength of the intersubband transition, $\hbar\omega_0$ its energy, m_0 the electronic mass, ε_0 the vacuum permittivity, and L_{eff} an effective QW thickness related to the confinement of the electronic wavefunctions. The damping Γ is a phenomenological factor, nominally equivalent to the transition FWHM. The oscillator strength is related to the dipole matrix element d between the envelope functions of the two subbands: $f = (2m_0/\hbar)\omega_0 d^2$. In our case a value d = 1.9 nm was computed using the proper orthonormalization procedure. Figure 3 reports TM reflectance curves calculated in this way for various incidence angles. This simple linear-dispersion model reproduces remarkably well the measured data, and correctly describes the anti-crossing behavior and polariton splitting. This should not surprise in view of the known equivalence of the semiclassical and quantum description of coupled harmonic oscillators. The value of the vacuum-field Rabi splitting can be tuned to the observed one by fitting the confinement length L_{eff}. This yields L_{eff} = 7.8 nm, as expected a thickness slightly larger than the well width.

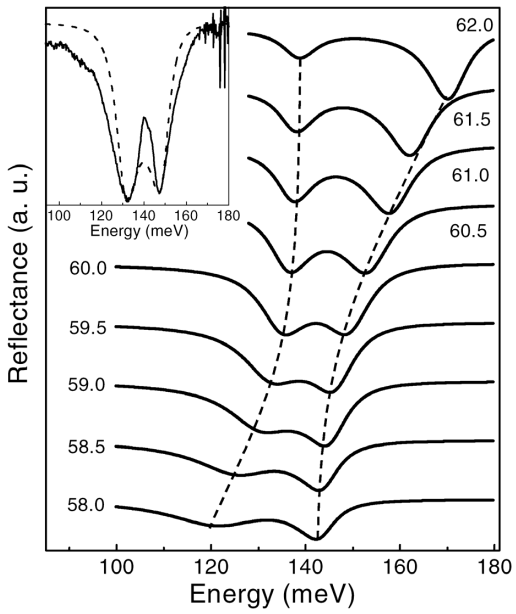

Figure 3 TM reflectance of the sample as obtained at different incidence angles using the simulation procedure described in the text. In the inset we report a comparison between the experimental and calculated spectrum at the resonance angle of 60.05°.

References

[1] S. Haroche and D. Kleppner, Phys. Today **42**, No. 1, 24 (1989).
[2] J. M. Raimond, M. Brune, and S. Haroche, Rev. Mod. Phys. **73**, 565 (2001).
[3] C. Weisbuch, M. Nishioka, A. Ishikawa, and Y. Arakawa, Phys. Rev. Lett. **69**, 3314 (1992).
[4] A. Tredicucci *et al*., Phys. Rev. Lett. **75**, 3906 (1995).
[5] M. Saba *et al*., Nature **414**, 731 (2001).
[6] H. Deng, G. Weihs, C. Santori, J. Bloch, and Y. Yamamoto, Science **298**, 199 (2002).
[7] A. Liu, Phys. Rev. B **55**, 7101 (1997).
[8] D. Dini, R. Köhler, A. Tredicucci, G. Biasiol, and L. Sorba, Phys. Rev. Lett. **90**, 116401 (2003).

ELECTRONIC TRANSPORT IN HYBRID NORMAL-SUPERCONDUCTOR NANOSTRUCTURES

Francesco Giazotto, Pasqualantonio Pingue, Fabio Taddei, Rosario Fazio, Fabio Beltram

Heterostructures are now well established as the most dynamic and rapidly growing field of semiconductor research. This success stems mostly from the great freedom they offer in the design of material band diagram. With respect to bulk structures these additional possibilities derive from the addition of two elements: the "opaque" barrier (employed to realize quantum wells and other reduced-dimensionality systems, hot-electron injectors, and various heterojunction transistor) and the "thin" barrier (employed in order to obtain the tunnel effect - resonant and non resonant - and superlattices). The addition of a *superconducting barrier* (S) opens the way to the introduction of an entirely new effect in the physics of the heterostructures: *Andreev reflection* [1]. Andreev reflection allows the control of the nature and the phase of quasi-particles in the heterostructure (see Fig. 1(a)): an electron injected from the normal region (N, in our case a degenerate semiconductor) with energy lower than the superconductor energy gap Δ can not propagate as a single particle and can be *reflected* as a phase-matched "hole" (in the Fermi sea of the N region), while a Cooper pair is transmitted in the superconductor. All this has to be contrasted to normal reflection present also in non-superconducting heterostructures (Fig. 1(b)).

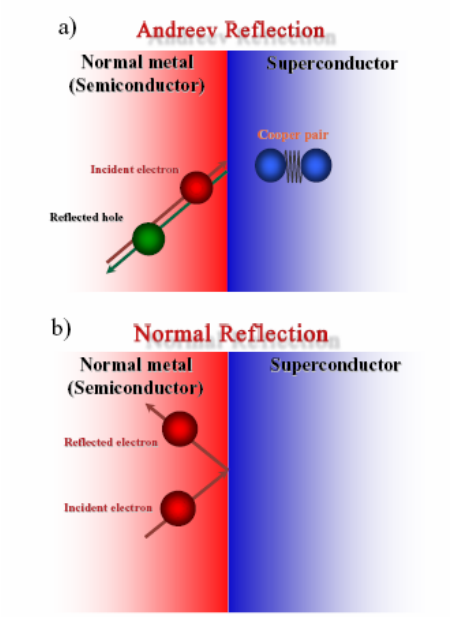

Figure 1 (a) Sketch of the Andreev reflection process: an electron impinging at the NS interface with subgap energy is retro-reflected as a hole that retraces the incoming electron time-reversed path. This process transfers a Cooper pair in S. **(b)** Scheme of normal reflection: no charge is transferred to the superconductor region.

Due to its two-particle nature, Andreev reflection is strongly affected by the transmissivity at the NS interface. High transparency is therefore required to observe this effect. The control of interface quality, particularly in the case of hybrid superconductor-semiconductor junctions is still a challenging task and much effort has to be devoted to its optimization.
Andreev reflection opens the way to the creation of new exotic electronic states and adds further flexibility to heterostructure research and applications. One particularly interesting case is that of a single scatterer represented by an insulating barrier (I) inserted in the structure during growth in the normal region. This configuration can give rise to controlled interference effects. Among these, one of the most intriguing is represented by de Gennes-Saint-James resonances [2] in NINS systems: multiple reflections off the superconductor gap (i.e. Andreev reflections) and the insulating barrier (i.e. normal reflections) can give rise to quasi-bound states that manifest themselves as conductance resonances. This process is the analogous of the ordinary resonant tunneling in normal double barrier structures.
We have been active in the field of hybrid superconducting nanostructures for some time and different material combinations and original fabrication protocols were explored and demonstrated [3,4], also in collaboration with TASC-INFM Laboratory. Here we present in particular the demonstration of the de Gennes-Saint-James (dGSJ)-type resonances in a microstructure consisting of a Nb/GaAs/AlGaAs/GaAs hybrid heterojunction [5].
A sketch of the Nb/GaAs/AlGaAs structure designed for this study is shown in Fig. 2(a). The semiconductor portion, grown by molecular beam epitaxy (MBE) at the TASC-INFM Laboratory in Trieste, consists of an $Al_{0.3}Ga_{0.7}As$ barrier embedded between GaAs layers. The top GaAs layers were heavily doped with a sequence of δ-doped layers in order to achieve a high-transparency contact with the superconductor. An amorphous As cap layer was deposited in the MBE growth chamber to protect

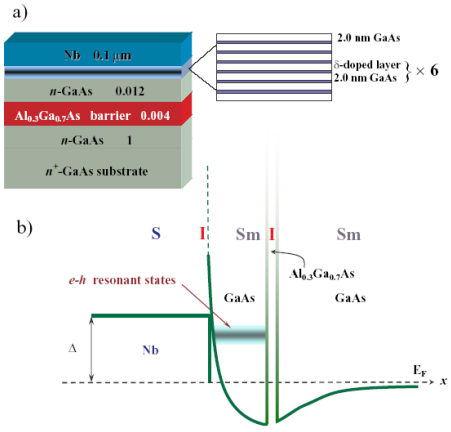

Figure 2 (a) Schematic structure of the Nb/GaAs/AlGaAs system analyzed here. **(b)** Sketch of the energy-band diagram of the structure. The shaded area represents de Gennes-Saint-James quasi-bound state confined between the superconductor and the $Al_{0.3}Ga_{0.7}As$ barrier.

the surface during transfer in air to an UHV sputter-deposition/surface analysis system at NEST. After thermal desorption of the As protective cap layer, the Nb film was deposited *in situ* by sputtering. The thickness of the GaAs epilayer sandwiched between the superconductor and the AlGaAs barrier was selected in order to have an experimentally-accessible single de Gennes-Saint-James quasi-bound state below the superconductive gap, and δ-doped layers at the Nb/GaAs interface were employed to achieve the required transmissivity and maximize Andreev reflection. A reference structure was also grown which consisted of a Nb/δ-doped-GaAs junction *without* the AlGaAs insulating barrier. A qualitative sketch of the energy-band diagram of our structure is depicted in Fig. 2(b). The same figure also shows the electron-hole (*e-h*) dGSJ resonance that develops between the superconductor and normal barriers.

Figure 3 shows the measured differential conductance *vs* bias ($G(V)$) for the resonant structure (panel (a)) and for the reference semiconductor-superconductor (SmS) junction (SmS structure, panel (b)) at $T = 0.34$ K. Comparison of the two characteristics clearly shows the presence of a marked subgap conductance peak in the SmISmS, resonant device. This result is the first demonstration of dGSJ resonant transport in a hybrid SSm system. The resonance is superimposed to the typical Andreev-dominated subgap conductance. The symmetry of conductance and the zero-bias conductance peak peculiar to "reflectionless tunneling" [6] further demonstrate the effectiveness of the fabrication protocol.

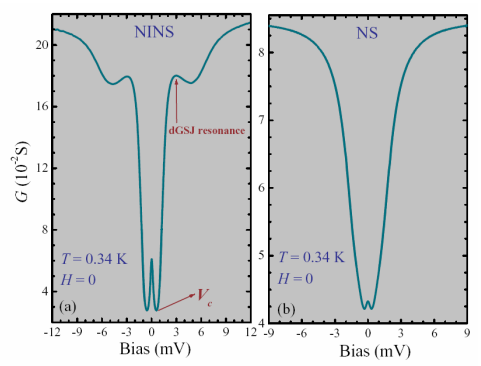

Figure 3 Differential conductance *vs*. voltage at T=0.34 K for the NINS junction, **(a)**, and for the reference NS junction, **(b)**. Both curves show reflectionless tunneling enhancement around zero bias. In (a) a finite-bias, subgap de Gennes-Saint-James peak is present.

Quantitative determination of the resonant transport properties in such system is not trivial as can be inferred by inspecting Fig. 2(b) and considering the diffusive nature of the normal regions. dGSJ enhancement, however, is an intrinsically ballistic phenomenon so that its essential features can be captured with relative ease. From the analysis of the zero-bias conductance peak it is possible to obtain information about some properties of the structure, as for example, the series resistance that may alter the correct energy position of the resonance. The width of the reflectionless tunneling peak, V_c (see Fig. 3(a)), is of order of the Thouless energy of the system [6] (i.e., the typical correlation length for disordered conductors) $E_{Th}=\hbar D/L_T^2$, where L_T is the thermal coherence length and D the diffusion constant. From the comparison of the theoretical and the experimental values for V_c we were able to extract the series-resistance contribution to the conductivity.

A simple one-dimensional NINS ballistic model can capture the essential features of this system, namely the number and position of resonances as a function of separation of the insulating barrier from the superconductor. By including the series resistance contribution determined above and from the theoretical energy position of the resonance calculated with the parameters of the structure, we

demonstrated that the observed effect is to be interpreted in terms of dGSJ-resonant transport. Ordinary resonant tunneling in the normal double-barrier potential schematically shown in Fig. 2(b) can not explain the observed subgap structure. This is indicated by the symmetry in the experimental data for positive and negative bias and is further proven by the observed strong temperature and magnetic field dependence of the differential conductance (data not shown).
The present results show that the Nb/GaAs/AlGaAs system is a good candidate for the implementation of complex mesoscopic hybrid structures that can take advantage of the mature AlGaAs nanofabrication technology.

Another significant issue studied is related to heat transport in such hybrid superconducting nanostructures. As a matter of fact heat transport through metal-superconductor interfaces can be applied to microcooling [7-9]. The physical mechanism underlying this electronic cooling is quite simple. When a normal metal (N) is brought in contact with a superconductor, quasi-particle transport is effective only at energies larger than the S gap (see Fig. 4(a)). In fact, owing to the existence of the gap in the energy spectrum of the superconductor, at a given bias across the SN system only electrons possessing energies higher than the gap match available single-particle states and can transfer into the S portion of the junction.

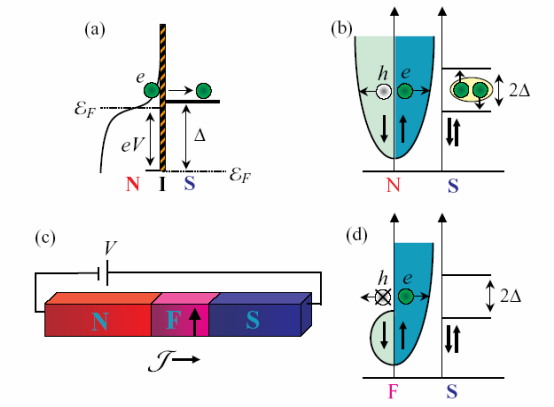

Figure 4 (a) Biasing the SIN junction around the energy gap Δ allows more energetic electrons *e* to tunnel into S, thus *cooling* the N electron population. **(b)** Schematic description of Andreev reflection at a NS contact. **(c)** Scheme of the proposed NFS microrefrigerator. The NF junction is supposed to be a highly transmissive electric contact. **(d)** Schematic representation of the principle of operation of the NFS microcooler. For spin polarization Π = 1, AR is hindered by the absence of available states for reflected holes, *h*. This subgap electron-transport suppression mechanism allows the operation of the microrefrigerator in the presence of efficient carrier transfer to S.

This selective transfer of "hot" carriers leads to the lowering of the effective electron temperature of the N electrode, even in the regime when electrons are thermally decoupled from the lattice. This situation can be experimentally realized with SN *tunnel* junctions where transport is dominated by quasi-particle dynamics. This unique property of Superconductor-Insulator-Normal metal (SIN) contacts was successfully employed for the realization of microcoolers [7-8]. Intrinsically, however, SIN devices present large values of the contact resistance (R_n) which hinder carrier transfer and lead to a severe limitation in the achievable cooling powers [8].
Decreasing R_n by using high-transparency interfaces is not a viable route to increase cooling power. At low R_n values, carrier transfer is made possible by Andreev reflection (AR) (see Fig. 4(b)) even at energies smaller than the energy gap. This does lead to increased conductivity, but does not contribute to thermal transport through the system.
We proposed a cooling mechanism alternative to traditional SIN junctions which proved highly efficient [10]. Our proposal is based on the use of a thin ferromagnetic layer (F) in good electric contact with S (Fig. 4(c)). The physical basis of the FS microcooler operation resides in the spin-band splitting characteristic of F. In fact the electron involved in AR and its phase-matched hole must belong to opposite spin bands; thus, suppression of the Andreev current occurs in an FS junction and its intensity depends on the degree of the F-layer spin polarization Π (Fig. 4(d)). In the limit of large Π and good metallic contact between the F and S electrodes, we observe a drastic suppression of the subgap current, while keeping efficient hot-carrier transfer leading to a considerable thermal flux 9. The predicted cooling power densities (up to 600 nW/μm^2) are almost two orders of magnitude larger than those of optimized SIN junctions (Fig. 5).

This efficiency enhancement translates into a dramatic reduction of the final achievable electron temperature. Half-metallic CrO_2/Al bilayers were indicated as ideal candidates for the implementation of the device. The well-developed CrO_2 technology can in fact be used to realize complex FS arrays coupled with normal electrodes for optimal device geometries.

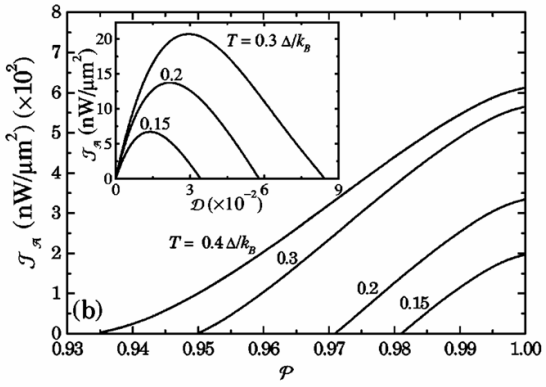

Figure 5 Maximum cooling-power surface density θ_A versus spin polarization Π for various temperatures. The inset shows the same quantity for a SIN junction as a function of contact transmissivity Δ.

References

[1] A. F. Andreev, Zh. Eksp. Teor. Fiz. **46**, 1823 (1964).
[2] P. G. de Gennes and D. Saint-James, Phys. Lett. **4**, 151 (1963).
[3] A. Badolato, F. Giazotto, M. Lazzarino, P. Pingue, F. Beltram, C. Lucheroni, and R. Fazio, Phys. Rev. B **62**, 9831 (2000).
[4] F. Giazotto, M. Cecchini, P. Pingue, F. Beltram, M. Lazzarino, D. Orani, S. Rubini, and A. Franciosi, Appl. Phys. Lett. **78**, 1772 (2001).
[5] F. Giazotto, P. Pingue, F. Beltram, M. Lazzarino, D. Orani, S. Rubini, and A. Franciosi, Phys. Rev. Lett. **21**, 216808 (2001).
[6] C. W. J. Beenakker, Rev. Mod. Phys. **69**, 731 (1997).
[7] M. Nahum, T. M. Eiles, and J. M. Martinis, Appl. Phys. Lett. **65**, 3123 (1994).
[8] M. M. Leivo, J. P. Pekola, and D. V. Averin, Appl. Phys. Lett. **68**, 1996 (1996).
[9] J. P. Pekola, D. V. Anghel, T. I. Suppula, J. K. Suoknuuti, A. J. Manninen, and M. Manninen, Appl. Phys. Lett. **76**, 2782 (2000).
[10] F. Giazotto, F. Taddei, R. Fazio, and F. Beltram, Appl. Phys. Lett. **80**, 3784 (2002).

VISUALIZATION OF PROTEIN TRAFFICKING AND PROTEIN-PROTEIN INTERACTIONS IN LIVING CELLS

Aldo Ferrari, Antonio Fittipaldi, Caterina Arcangeli, Arianna Sabò, Vittorio Pellegrini, Alessandro Marcello, Fabio Beltram, Mauro Giacca

In the world of life sciences, one of the critical issues of the post-genomic era is the understanding of protein function, protein dynamics and protein-protein interaction. While molecular biology and biochemistry allow the study of some of these topics in vitro, novel techniques are clearly required to tackle these problems inside the living cells.
In the framework of the NEST activities, one of the goals is the development and exploitation of novel optical nanobiotechnologies for the study of protein function. This goal is pursued through a multidisciplinary approach, which includes expertise in molecular biology and biomolecular physics and entails high-resolution and high-sensitivity imaging and spectroscopy to visualize, in real time, biological macromolecules labelled with fluorescent probes or quantum dots in living cells.

Dissection of protein-protein interactions at the HIV-1 promoter using fluorescence resonance energy transfer (FRET)

This research project has so far addressed the study of some of the properties of the Tat protein of the human immunodeficiency virus type 1 (HIV-1). After infection of the target cells, the viral RNA of HIV-1 is reverse-transcribed and integrated into the host genome. Upon integration, and independent from the integration site, the proviral DNA sequence is organized in a chromatin structure that exerts a repressive role on transcription; repression is overcome by a variety of extracellular stimuli that lead to cellular activation. Persistence of the virus as an integrated, transcriptionally silent provirus in specific cellular reservoirs allows the infected cells to escape from the current antiretroviral therapies and the infection to rebound after discontinuation of treatment. Therefore, the understanding of the molecular mechanisms controlling silencing and reactivation of the HIV-1 provirus at its integration site within the host cell genome has profound implications for both the elucidation of the HIV disease pathogenesis and for its pharmacological control.
The most powerful activator of HIV-1 gene expression is the viral Tat transactivator. Tat is a small polypeptide (of 101 amino acids in most viral strains) that interacts with a cis-acting RNA element (trans-activation-responsive region, TAR, present at the 5' end of all viral mRNAs; nt +1 to +60; for a recent review on Tat see: [1]). From here, Tat induces a modification of chromatin at the HIV-1 LTR promoter and stimulates the recruitment of elongation-competent RNA polymerase II complexes capable of processive transcription. These activities require the coordinate assembly of multiprotein cellular complexes onto the promoter, a process that we have started to physically dissect by studying the interactions of multiple protein pairs using fluorescent resonance energy transfer (FRET).
FRET exploits radiationless energy transfer driven by dipole-dipole interaction occurring from a fluorophore (the donor) in the excited state to another fluorophore (the acceptor) when in close proximity; energy transfer is followed by acceptor fluorescence [2,3]. Among the fluorophore pairs with spectral characteristics optimal for FRET are those formed by some variants of the green fluorescent proteins (GFP), namely the CFP (cyan)/YFP (yellow) and the BFP (blue)/EGFP (green) pairs. Technically, the visualization of fluorescence from ECFP/EYFP is easier, due to the higher temporal stability of the photon emission associated with the reduction of photobleaching effects. However, the determination of FRET efficiency between these two proteins requires careful measurement due to the extensive overlapping of their emission spectra [4,5]. In contrast, the emission of BFP and EGFP overlaps only minimally. Thus, the FRET efficiency can be calculated as a simple ratio of the emission intensities of the acceptor excited within its absorption band and at resonance with the donor absorption [6]. The visualization of BFP-tagged proteins, however, is difficult when compared to other GFP-fusion proteins as the BFP rapidly converts to a dark (non-emissive) state after photoexcitation. FRET presents several advantages in comparison with other techniques employed to detect protein-protein interactions. Firstly, the simple co-localization of two proteins is not sufficient to yield energy transfer: the presence of FRET actually indicates protein-protein interaction at distances of a few nanometers for many pairs of optically matched fluorophores. Secondly, the use of gene-encoded GFP variants allows the visualization of interactions in real time and in living cells. Thirdly, FRET actually determines not only "whether" but also "where" proteins interact inside the nucleus.

This is of particular value, especially given the increasing importance ascribed to the compartmentalization of biological processes in vivo, as also outlined above.
One of the cellular partners of Tat is Cyclin T1, a component of the P-TEFb kinase complex. Our current understanding suggests that Tat recruits P-TEFb to the viral LTR to promote transcriptional elongation of viral RNAs. FRET was mapped to different cellular compartments after transfection of Tat and Cyclin T1 tagged by optically matched variants of the green fluorescent protein. Strong energy transfer (implying direct protein-protein interaction at distances shorter than 10 nm) was observed between the two proteins both in the cytoplasm and in discrete regions of the nucleus overlapping with Tat localization.
Cyclin T1 is the cyclin partner of the CDK9 kinase forming the pTEFb complex, a key factor in the regulation of HIV transcription; unexpectedly, this complex was found to reside in specific compartments inside nucleus [6,7]. These pTEFb foci appear juxtaposed, although not exactly coincident, with nuclear speckles, while they co-localize with promyelocytic leukemia (PML) nuclear bodies [8]. In keeping with this observation, Cyclin T1 was found to specifically bind PML in FRET experiments. This interaction occurs via the carboxy-terminal portion of Cyclin T1, distal from the cyclin box and the Tat recognition motif, and involves the RBCC motif (RING + B-boxes + coiled-coil) of PML. These observations favor a model by which nuclear bodies modulate the activity of the HIV promoter by coordinating the availability of several factors that act in concert and are transiently

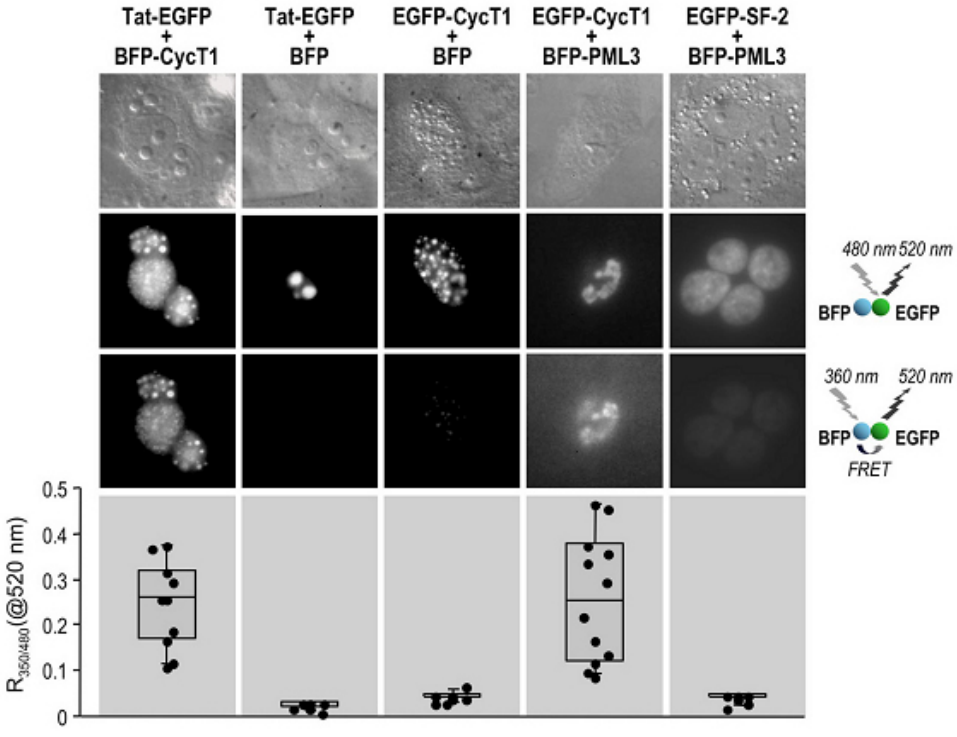

Figure 1 FRET analysis of protein-protein interactions in vivo.
Visualization of fluorescence resonant energy transfer (FRET). The plasmid constructs indicated on top of each column were transfected in HL3T1 cells; transfected cells were visualized by transmitted light in Nomarski configuration (upper panels), by excitation at 480 nm and collection at 520 nm, showing EGFP fluorescence after direct EGFP excitation (middle panels), and by excitation at 350 nm and collection at 520 nm, showing EGFP fluorescence after BFP excitation, indicating FRET (lower panels). Fluorescent emission at 520 nm from individual cells transfected with the indicated constructs was recorded after excitation at 350 or 480 nm, and integrated intensities over the whole cell were evaluated. Plotted values (indicated by dots) represent the ratio between these two measurements: higher values indicate more efficient resonant energy transfer between BFP and EGFP. Ten consecutively analysed cells were considered for each transfection; both their individual fluorescence ratio and their percentile box-plot distribution are shown. Horizontal lines of the percentile box plot distribution of FRET values, from top to bottom, mark the 10^{th}, 25^{th}, 50^{th}, 75^{th}, and 90^{th} percentile respectively.

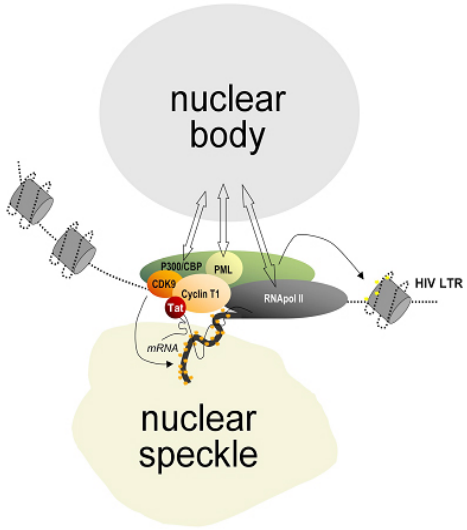

Figure 2 Model for the regulation of HIV-1 Tat-mediated transcriptional activation of the chromatinized HIV LTR promoter.
A snapshot of the HIV LTR transcriptional activation by Tat is taken. This highly dynamic process is shown in the act of recruiting some of the specific cellular co-factors that associate with Tat for efficient transcriptional activation of the integrated viral promoter. Center stage is taken by cellular RNA polymerase (RNAP II), which coordinates transcriptional and splicing processes through its carboxy-terminal (CTD) tail. HIV Tat associates TAR at the 5'-end of each transcript together with Cyclin T1. The latter recruits its cognate kinase, Cdk9, which enhances the processivity of RNAP II by phosphorylation of the CTD domain (orange asterisks). Tat also recruits the transcriptional co-activator and acetyl-transferase p300 to the chromatinized promoter allowing acetylation (arrows) of proximal histones and, possibly, of Tat itself (yellow asterisks). The timely availability of each of these factors to the HIV LTR is a regulated process. Part of this regulation is accorded by the trafficking of components to and from specific sub-nuclear compartments that are present in the cell nucleus (arrows). Nuclear speckles are rich in splicing factors that are involved in precursor mRNA processing, a process coordinated by the RNAP II CTD. On the other hand, nuclear bodies (NBs) coordinate the presence of factors such as p300 and Cyclin T1 through direct interactions of the PML protein.

part of the same complex assembled onto the LTR, including P-TEFb, p300/CBP, RNA polymerase II, and PML itself.

Intracellular and inter-cellular Tat trafficking

Besides having transcriptional functions at the HIV promoter, the Tat polypeptide is also unique in that it is released by expressing cells and enters non-producing cells when present in the extracellular environment [9,10]. Tat released by infected cells is likely to exert autocrine and paracrine activities with possible important implications for HIV disease pathogenesis. The capacity to cross cell membranes depends upon the integrity of the basic region of the protein, a 9-amino acid, arginine-rich sequence that also corresponds to the nuclear localization signal and the TAR-binding domain of the protein [1,11]. Mounting interest in the cell penetrating capacity of Tat is due to its ability to drive the internalization of large protein cargos that are chemically coupled or fused to it. In particular, the addition of the basic domain of Tat [12] or its crosslink [13] to heterologous molecules, even of a large size, mediates their cellular uptake; this property is currently widely exploited as a biotechnological tool for transcellular protein transduction.
Despite this variety of successful biotechnological applications of Tat as a delivery vector across cell membranes, the cellular mechanisms involved in the uptake of wild type HIV-1 Tat and of Tat fusion proteins are still obscure. We have observed that extracellular Tat specifically interacts with the heparan sulfate chains of cell membrane heparan sulfate proteoglycans (HSPGs) [14], and that this interaction is absolutely required for the uptake process to occur [15]. These results, together with the observation that the internalization of the fusion of large molecules to Tat is impaired at 4°C, suggest that an active endocytic process follows the interaction of Tat with HSPGs.
The Tat-containing endosomes were visualized at high resolution and in real time in living cells after treatment with a recombinant fluorescent protein containing Tat and GFP. Tat endosomes were found to accumulate at the cell membrane as early as 15 min following addition of the protein to the cell culture medium; each endosome was estimated to contain ~300 molecules of GPF-Tat. By time lapse microscopy visualization we tracked the movement of several individual vesicles; on average, they were found to proceed from the cell membrane to the nucleus with a linear movement at a velocity of 3 μm/h.
We also observed that GFP-labeled-Tat co-localizes in endosomes with the B-subunit of cholera toxin and with endogenous or transfected caveolin-1, but not with transferrin or with the early endosome

marker EEA1, an observation that excludes endocytosis in clathrin-coated vesicles as the mechanism for Tat internalization. Consistent with the association of caveolae with cell membrane lipid rafts, we also found that the Tat uptake was unaffected by treatment with Triton X-100 – which disrupts transferrin endosomes but not lipid rafts – and was impaired by cyclodextrin B, which extracts cholesterol from lipid rafts. Together these results clearly indicate that extracellular Tat is internalized by a mechanism involving caveolar endocytosis and originating from cell membrane lipid rafts.

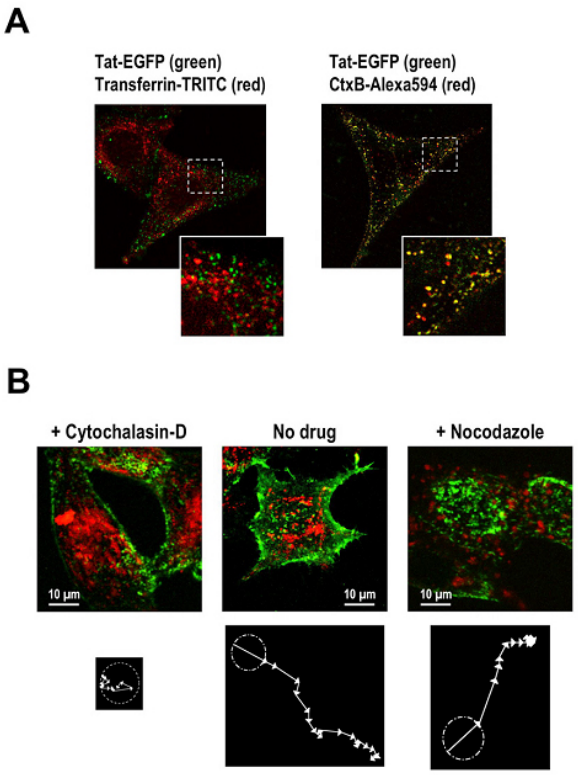

Figure 3 HIV-1 Tat is internalized through caveolar endocytosis
(A) Endosomes containing recombinant Tat fused to EGFP do not co-localize with those containing transferrin, a marker of chlatrin endocytosis (left side). In contrast, a vast proportion of Tat-EGFP endosomes also contain the B subunit of cholera toxin (yellow endosomes), a protein that is internalized by caveolar endocytosis.
(B) Maximum projections of a laser-scanning confocal fluorescence z recording (0.3 µm step) after the addition of Tat-EGFP (green) together with Transferrin-TexasRed (red) to HeLa cells treated with Cytochalasin-D or Nocodazole. The lower part shows vector tracks of typical Tat-EGFP vesicle trajectories (recorded every 15 minutes and followed up to 8 hours at 37 °C by wide-field fluorescence microscopy in the different conditions examined). Treatment with cytochalasin D, a drug known to impair caveolar endocytosis, freezes endosome movement in correspondence with the cell membrane. Nocodazole (disrupting microtubular trafficking) has no effect.

References

[1] A. Marcello, M. Zoppè, and M. Giacca, IUBMB Life **51**, 175.
[2] P. R. Selvin, Nat. Struct. Biol. **7**, 730.
[3] P. van Roessel and A. H. Brand, Nat. Cell Biol. **4**, E15.
[4] P. I. Bastiaens and R. Pepperkok, Trends Biochem. Sci. **25**, 631.
[5] J. Lippincott-Schwartz, E. Snapp, and A. Kenworthy, Nat. Rev. Mol. Cell. Biol. **2**, 444.
[6] A. Marcello, R. A. G. Cinelli, A. Ferrari, A. Signorelli, M. Tyagi, V. Pellegrini, F. Beltram, and M. Giacca, J. Biol. Chem. **276**, 39220.
[7] C. H. Herrmann and M. A. Mancini, J. Cell. Sci. **114**, 1491.
[8] A. Marcello, A. Ferrari, V. Pellegrini, G. Pegoraro, M. Lusic, F. Beltram, and M. Giacca, EMBO J. **22**, 2156 (2003).
[9] M. Green and P. M. Loewenstein, Cell **55**, 1179.
[10] A. D. Frankel and C. O. Pabo, Cell **55**, 1189.
[11] K. T. Jeang, H. Xiao, and E. A. Rich, J. Biol. Chem. **274**, 28837.
[12] H. Nagahara, A. M. Vocero-Akbani, E. L. Snyder, A. Ho, D. G. Latham, N. A. Lissy, M. Becker-Hapak, S. A. Ezhevsky, and S. F. Dowdy, Nat. Med. **4**, 1449.
[13] S. Fawell, J. Seery, Y. Daikh, C. Moore, L. L. Chen, B. Pepinsky, and J. Barsoum, Proc. Natl. Acad. Sci. USA **91**, 664.
[14] M. Rusnati, G. Tulipano, D. Spillmann, E. Tanghetti, P. Oreste, G. Zoppetti, M. Giacca, and M. Presta, J. Biol. Chem. **274**, 28198 (1999).
[15] M. Tyagi, M. Rusnati, M. Presta, and M. Giacca, M. J. Biol. Chem. **276**, 3254 (2001).

SPECTROSCOPY OF MAGNETO-ROTONS IN QUANTUM HALL FERROMAGNETS

Stefano Luin, Vittorio Pellegrini

Two-dimensional electron systems in quantizing magnetic fields exhibit a variety of collective phases [1]. The additional degree of freedom associated to layer occupation makes bilayer systems at total Landau level filling factor $\nu_T = 1$ particularly interesting [2]. At this filling factor a phase transition exists between incompressible and compressible phases (see inset of Fig. 1(a)). The incompressible phases are stable at large tunneling gaps Δ_{SAS} and/or low interlayer distances d. Compressible phases, characterized by the absence of the quantum Hall (QH) signature, emerge at large d and low Δ_{SAS}. The phase transition is finely tuned by the interplay between Δ_{SAS} with intra- and inter-layer Coulomb interactions. In the incompressible phases the different dependence of depolarization and excitonic terms on wave-vector produce, at $|\mathbf{q}| = q > 0$, a magnetoroton (MR) minimum in the dispersion of the charge-density tunneling excitation (CDE). In current theories the incompressible–compressible phase transition is linked to an instability due to softening of a MR of CDE modes [3,4,5]. Recent experimental results on ground state properties close to the phase boundary were focused on Coulomb drag and interlayer tunneling at very low values of Δ_{SAS} [6]. These studies suggested the appearance of a Goldstone mode in the incompressible phase and offered evidence of superfluid behavior. Experiments that probe dispersive collective excitations and their softening as a function of Δ_{SAS} and d could provide direct evidence of the impact of excitonic terms of interactions in the quantum phase transitions of the bilayers at ν_T=1.

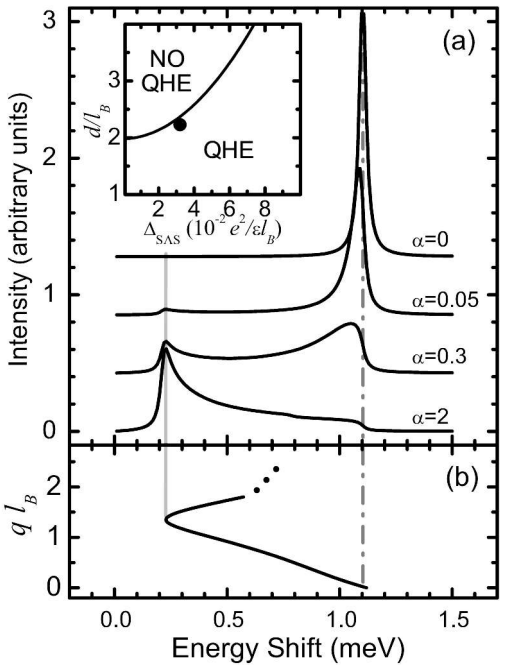

Figure 1 (a) Calculated inelastic light scattering spectra. α labels the breakdown of wavevector conservation (see text). The curves are the response functions calculated in TDHFA using the dispersion shown in panel **(b)**, for a sample close to the phase transition (phase diagram in inset of (a)).

In previous experiments, resonant inelastic light scattering methods were employed to access q~0 soft tunneling spin excitations at even values of ν_T [7]. Here we review our recent work in collaboration with Aron Pinczuk (Columbia University and Bell Laboratories) and Loren Pfeiffer (Bell Laboratories). In the experiments reported here resonant inelastic light scattering is employed to probe the low-energy CDE of bilayer QH ferromagnets at ν_T=1 in states close to a incompressible–compressible phase boundary [8]. These experiments seek direct evidence of soft MR modes with q~1/l_B (l_B is the magnetic length), and attempt to uncover the impact of excitonic terms of interactions in the quantum phase transitions of the ν_T=1 bilayer systems. These resonant inelastic light scattering experiments take advantage of breakdown of wave-vector conservation that occurs in the QH state due to residual disorder. This aspect of light scattering methods offers experimental access to critical points in the mode dispersion such as the one at the MR minimum. To gain further insight from the data, the results are compared to time-dependent Hartree-Fock (TDHF) calculations [9] of light scattering intensities. The evaluations incorporate effects of breakdown of wave-vector conservation [10], as well as the resonant enhancement. This simplified model successfully reproduces both MR energies and light scattering lineshape. This success indicates that the sharpening of the MR spectral lineshape follows from remarkable

changes in the mode dispersion and matrix elements near the incompressible–compressible phase boundary. These results uncover significant evidence that softening of rotons play major roles in the phase transitions of bilayers at ν_T=1, and suggest a leading role for excitonic Coulomb interactions in transitions between these highly correlated phases.

To highlight the impact of breakdown of wavevector conservation we focused on a sample in close proximity to the phase boundary (see the dot in the inset of Fig. 1(a)) for which the calculated dispersion is shown in Fig. 1(b). The dispersion is characterized by a deep MR which anticipates the occurrence of a continuous quantum phase transition. We note that TDHFA being a mean-field theory fails to reproduce the collective mode dispersion when q >> $1/l_B$. That part of the dispersion was not included in the model. The intensity of inelastic light scattering is in the lowest order approximation proportional to the dynamic structure factor $S(q,\omega;\alpha)$. Here α is a phenomenological broadening parameter in wavevector space, introduced by Marmorkos and Das Sarma [10] to account for the effects of disorder in the breakdown of wavevector conservation. Figure 1(a) shows the calculated inelastic light scattering spectra. In these calculations a broadening factor Γ=0.035 meV, due to lifetime limited by disorder and impurity scattering, was also considered [10]. Further details on the results of the calculations can be found in Ref.[8]. Figure 1(a) shows that small values of α, of the order of $0.1\cdot 1/l_B$, are sufficient to yield significant intensity at the energy of MR critical point. This is due to the fact that the matrix element $|M(q)|^2$ that enters the dynamic structure factor and acts as the oscillator strength for inelastic light scattering tends to peak sharply at the MR wavevector when the bilayer approaches the phase transition instability [8].

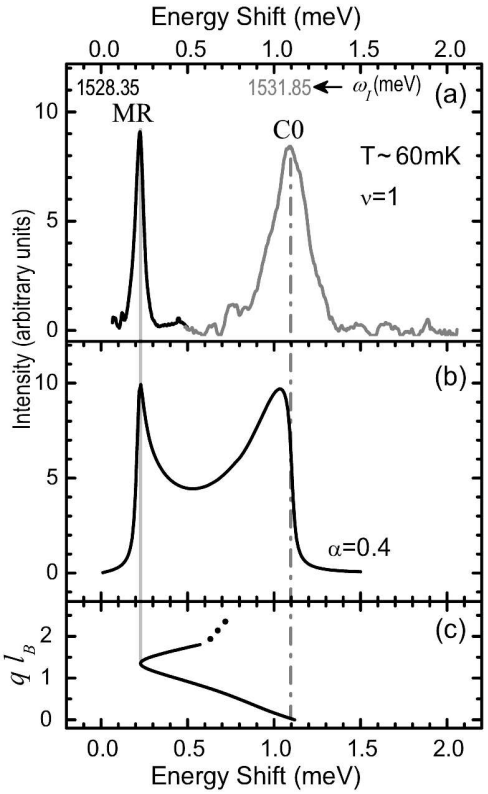

Figure 2 (a) Experimental MR and C0 resonant Raman peaks, for two different incident photon energies (reported in the figure). Background is subtracted. **(b)** Response function for a chosen value of α=0.4. **(c)**: collective mode dispersion for different values of α.

Figure 2 allows us to compare measured spectra (a) with calculations in which α is set at 0.4 (b). The sample is characterized by a 7.5-nm-wide $Al_{0.1}Ga_{0.9}As$ barrier, electron density $n=1.2\cdot 10^{11}cm^{-2}$ and Δ_{SAS} = 0.32 meV and its position in the phase diagram corresponds to the dot in the inset of Fig.1(a). A value of α= 0.4 yields an effective length scale of ~ $3l_B$ for the terms in the disorder potential responsible for the breakdown of wavevector conservation. The resonant inelastic light scattering spectra are obtained at two different incident photon energies and displayed after conventional subtraction of background due to laser and magneto-luminescence. The assignments of the two spectral features to CDE at q=0 (C0) and to the MR are consistent with the calculated dispersion shown in Fig. 1(b) and Fig. 2(c). The calculation reproduces the energy position and the widths of the peaks. The fact that the C0 width is larger than that of the MR is significant and reflects the peculiar behavior of the $|M(q)|^2$ factor close to the phase boundary. On the contrary, results obtained from a sample far from the phase boundary show a broad and weak MR peak (compared to C0) and located at higher energies (≈0.6 meV) [8]. The calculated spectra shown in Fig. 2 differ from the measurements in the region between the C0 and MR modes. The discrepancy could be related to differences in resonant enhancements.

These results are significant because they suggest that roton softening plays a major role in the incompressible–compressible phase transitions of the bilayers at $\nu_T = 1$. The interactions that drive the transition are related to the excitonic Coulomb term that creates the roton in the CDE mode dispersion. Such excitonic binding increases at lower values of Δ_{SAS} due to enhanced overlap between the single-particle wavefunctions of symmetric and antisymmetric states. The results presented here thus suggest a leading role of excitonic Coulomb interactions in transitions between highly correlated phases. The results are consistent with a scenario in which the instability is associated with the condensation of neutral excitons, a subject of current interest in bilayers and in other semiconductor systems [6,11].

Collaborations

This activity is carried out in collaboration with Bell Laboratories, Murray Hill, NJ, USA and Columbia University, New York City, NY, USA.

References

[1] R. E. Prange and S. M. Girvin (Eds.): *The Quantum Hall Effect* (Springer-Verlag, New York, 1987).

[2] S. M. Girvin and A. H. MacDonald in: A. Pinczuk and S. Das Sarma (Eds): *Perspectives in Quantum Hall Effect* (Wiley, New York, 1997) chapter 5, p.161.

[3] L. Brey, Phys. Rev. Lett. **65**, 903 (1990).

[4] A. H. MacDonald, P. M. Platzman, and G. S. Boebinger, Phys. Rev. Lett. **65**, 775 (1990).

[5] Y. N. Joglekar and A. H. MacDonald, Phys. Rev. B **65**, 235319 (2002).

[6] I. B. Spielman, J. P. Eisenstein, L. N. Pfeiffer, and K. W. West, Phys. Rev. Lett. **84**, 5808 (2000); I. B. Spielman, J. P. Eisenstein, L. N. Pfeiffer, and K. W. West, Phys. Rev. Lett. **87**, 036803 (2001); M. Kellogg, I. B. Spielman, J. P. Eisenstein, L. N. Pfeiffer, and K. W. West, Phys. Rev. Lett. **88**, 126804 (2002).

[7] V. Pellegrini, A. Pinczuk, B. S. Dennis, A. S. Plaut, L. N. Pfeiffer, and K. W. West, Phys. Rev. Lett. **78**, 310 (1997); V. Pellegrini, A. Pinczuk, B. S. Dennis, A. S. Plaut, L. N. Pfeiffer, and K. W. West, Science **281**, 799 (1998); V. Pellegrini, A. Pinczuk, Solid State Commun. **119**, 301 (2001).

[8] S. Luin, V. Pellegrini, A. Pinczuk, B. S. Dennis, L. N. Pfeiffer, and K. W. West, Phys. Rev. Lett. **90**, 236802 (2003).

[9] Daw-Wei Wang, S. Das Sarma, E. Demler, and B. I. Halperin, Phys. Rev. B **66**, 195334 (2002).

[10] I. K. Marmorkos and S. Das Sarma, Phys. Rev. B **45**, 13396 (1992).

[11] L. V. Butov, Solid State Commun. **127**, 89 (2003); D. Snoke, Y. Liu, S. Denev, L. N. Pfeiffer, and K. W. West, Solid State Commun. **127**, 187 (2003).

MOLECULAR MODELING AND SPECTROSCOPY OF FLUORESCENT PROTEINS

Riccardo Nifosì, Valentina Tozzini, Aldo Ferrari, Caterina Arcangeli, Vittorio Pellegrini, Paolo Giannozzi, Teodoro Laino, Mauro Giacca, Fabio Beltram

Fluorescent proteins are fascinating nanoscale systems which are often used in cell biology as visible tags for proteins of interest. The first of these fluorophores to be studied, the Green Fluorescent Protein (GFP) from the jellyfish Aequorea Victoria, is now considered only one member of an expanding class of fluoro- and chromo-proteins found in various organisms such as corals and sea anemones. Optimization of these probes for applications either as biological tags and sensors or for nanoscale photonic devices relies on understanding their photophysics. Here we report a combined experimental and theoretical study of a GFP mutant, with the aim of understanding some aspects of its complex photophysics and evaluate its suitability as a building block of optical storage with high density.
GFP owns its fluorescence to a small molecular fragment called chromophore which is positioned in the middle of the β-can fold of the protein (see Ref. [1] for reviews on the subject). The chromophore is formed spontaneously after the folding of the amino-acid chain, as a consequence of the cyclization of three subsequent amino acids (Serine, Tyrosine and Glycine in wild type GFP). The completely autocatalytic formation of the chromophore is the key reason for GFP success. Moreover, it was shown that by mutating the amino acid sequence it is possible to tune GFP fluorescence, and obtain, beside green, also blue, cyan and yellow light emitters. In addition to its interest for biological applications, GFP displays a very intriguing photophysics. Ultra-fast spectroscopy and single-molecule experiments

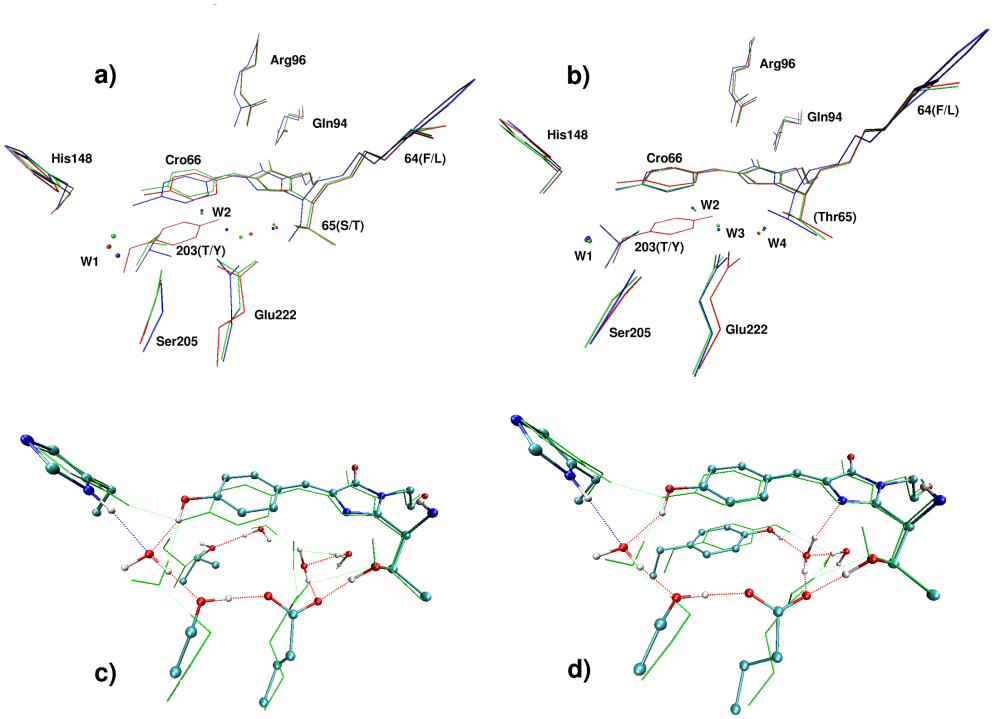

Figure 1 (a) Comparison between the crystal structure of WT (PDB code 1emb) (blue) and the minimized average MD structures of EGFP state A (green) and E^2GFP state A (red). Hydrogen atoms are not shown. **(b)** Comparison between the MD structures of the B states of S65T (blue), EGFP (green) and E^2GFP (red). **(c)** Comparison between the minimized average MD structures of EGFP state A (atom code color) and EGFP state B (in green). Only polar hydrogen atoms are shown. **(d)** Same as (c) for the E^2GFP mutant. All structures are superimposed on the α-carbons of the backbone.

revealed the presence of dark (i.e. non-fluorescent) states to and from which the protein undergoes transitions either spontaneously or as a consequence of light excitation. A deeper understanding of these aspects should help in the design of GFP mutants to either suppress or use the dark states as desired. There is currently an important research effort to investigate device applications of biomolecules. GFP fluorescence, detectable at the single molecule level [2,3], holds great promise for photonics at the nanoscale.

As is the common behavior of fluorophores, GFP photobleaches after a number of photon absorption-emission cycles. Photobleaching hinders biological applications where the tagged protein should be followed with high resolution for long periods (minutes, hours). Guided by previous studies of on/off switching of fluorescence in yellow mutants of GFP [2], we demonstrated recovery of fluorescence after photobleaching in a new mutant that was patented together with the related architecture for ultrahigh density information storage [3]. This variant, termed E^2GFP, carries the following mutations: F64L, S65T and T203Y (the single-letter code for amino acids is used and the number indicates the position in the sequence), i.e. a single point mutation with respect to commercial EGFP. E^2GFP single molecules can be switched off by intense irradiation at 476 nm and then switched back to the on state by irradiation at 350 nm. Photoinduced recovery of fluorescence can be exploited in biological experiments where a longer detection period is required or in other schemes where a nanoscopic portion of the cell is selectively unbleached after photobleaching of the whole region in order to follow the diffusion of a small number of GFP-tagged proteins. In addition, the optically controllable bistability of E^2GFP can be used to store and manipulate data at the single molecule level, where a (0,1) bit is encoded by the on and off states of the protein.

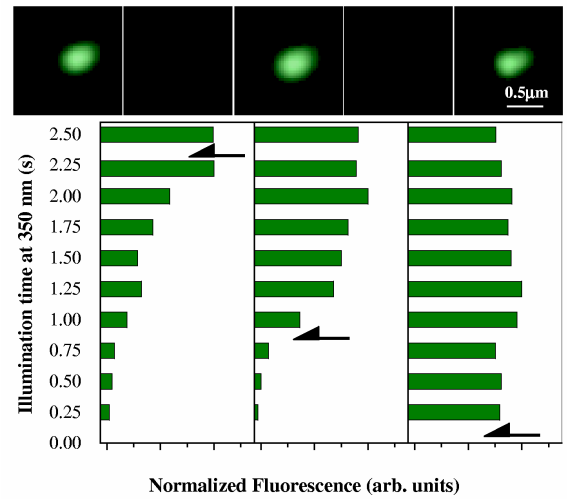

Figure 2 On/off switching operations illustrated by a series of experiments performed on clusters of E^2GFP molecules trapped in polyacrylamide PAA gel films (10 μm thick). The upper panel shows a representative sequence of E^2GFP switching behavior, with photoactivation times of 2.5 s, 1 s, and 250 ms (from the left to the right) at 350 nm (60 kW/cm^2). Off switching processes are accomplished by 7.7 s excitation at 476 nm (1 kW/cm^2). The green histograms in the lower panel report the integrated fluorescence intensity of E^2GFP clusters after 350 nm laser illumination at different laser powers: 0.05mW (0.6 kW/cm^2, leftmost panel), 0.14 mW (1.8 kW/cm^2, center panel), and 4.6 mW (60 kW/cm^2, rightmost panel) as a function of irradiation time (from 0.25 to 2.5 s). E^2GFP molecules were imaged by an intensified charge coupled device (CCD) camera (0.1 s integration time) during irradiation at 476 nm. Black arrows indicate the irradiation times for efficient photoconversion as deduced from the data in solution.

In order to further optimize the photoconversion efficiency also in different environment conditions it is necessary to understand the molecular mechanism of the on/off switching of fluorescence. Within this objective, we investigated the photoconversion process by spectroscopy both in solution and at the single molecule level and performed a theoretical modeling of the protein. The latter started with a molecular dynamics (MD) study of E^2GFP and of another variant, EGFP (F64L/S65T), which is commonly employed in molecular biology experiments and differs from E^2GFP by a single mutation [4]. Through this study we modeled the structure of the two mutants which were not available from X-ray experiments. We used (classical) MD simulations to investigate how the introduced mutations produce local rearrangements with respect to the structure of wild type GFP and of the single S65T mutant. The resulting configurations are shown in Fig. 1. With the aid of additional free-energy calculations we were able to understand the contribution of the mutated amino acids in the equilibrium between the neutral and anionic forms of the chromophore within the protein matrix. In particular, S65T is known to shift

the equilibrium away from the A state (with the neutral chromophore) in favor of the B state (with the anionic chromophore) because Threonine at position 65 is less efficient than Serine in solvating the negative charge on Glutamic acid at 222 (it is commonly accepted that E222 is anionic in the A state and neutral in the B state). We were able to attribute such difference to the hydrophobic interactions of T65 methyl substituent with surrounding non-polar groups. These interactions bring the hydroxyl of T65 away from E222 resulting in a weaker hydrogen bond that destabilizes the A state. The additional T203Y mutation in E^2GFP hinders the anionic state because it subtracts a hydrogen-bond donor to the phenolate of the chromophore. As a result, the B state is less populated in E^2GFP than in EGFP, and the equilibrium is shifted towards the A state.

The molecular dynamics study also provided the starting configurations for a quantum mechanics study on the chromophore in its immediate environment. We performed Density Functional Theory (DFT) calculations on systems including, beside the chromophore, two water molecules and some neighboring residues (Q94, R96, H148 and Y203/T203) [5]. These calculations helped to clarify how each residue interacting with the chromophore affects its vibrational frequencies and the excitation energy. We found that the excitation energies of the simulated systems show a linear relationship with the length of those bonds that change nature (i.e. single to double and vice versa) in going from one possible resonant structure of the chromophore to another, namely from the benzenoid to the quinonoid [6]. The experimental evidence for this relationship comes from previous Raman measurements performed on the isolated chromophore and on several GFP mutants [7]. It was found that the frequency of a high-frequency Raman peak correlates linearly with the absorption energy. The frequency of this mode probes the mixing between the resonant forms of the chromophore, because its

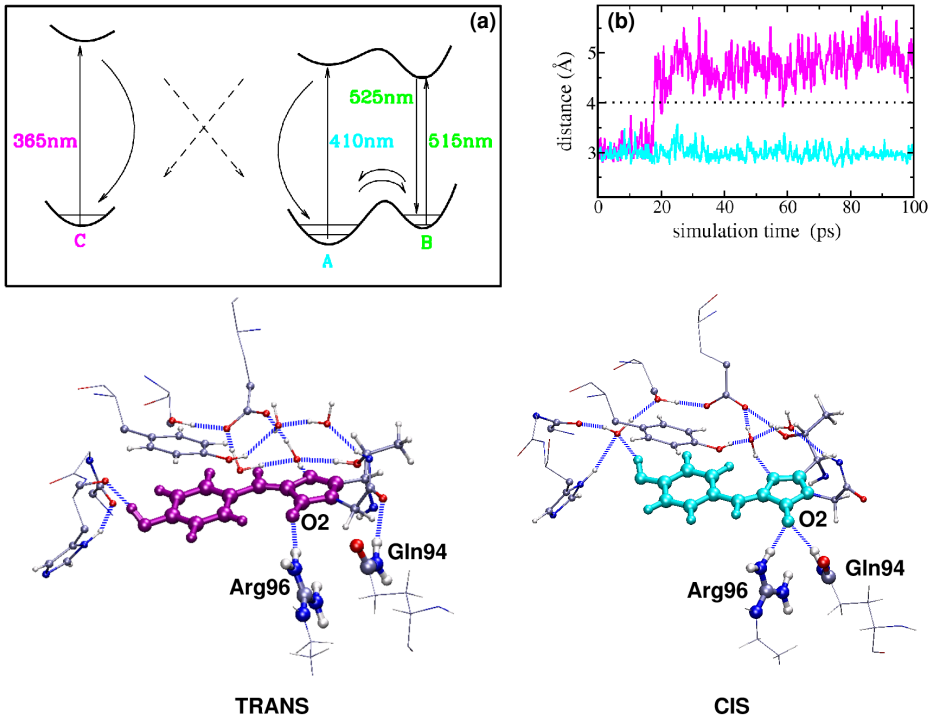

Figure 3 (a) Schematic representation of the three main states in E^2GFP. Vertical arrows represent absorption/emission processes between vibrational levels in ground and excited states. Dashed arrows are used to indicate the transition process between bright and dark states. A ground state barrier crossing between A and B is also indicated. **(b)** Distance between O2 of the chromophore and the donor of Q94 reported during the first 100 ps of the simulation for the trans state (magenta line) and of the cis state (cyan line), the sudden increase in the distance indicating the breaking of the hydrogen bond. Lower panel: structures of the chromophore and its environment in E^2GFP for neutral cis state (right) and neutral trans state (left) as obtained from molecular dynamics simulations.

pattern of vibration involves stretching of those bonds which characterize the two resonant forms. We calculated the vibrational spectrum of the chromophore in the environment and found a good agreement with the experimental measurements in the high-frequency range (1000-2000 cm^{-1}). The low-frequency range (500-1000 cm^{-1}) was investigated in connection with surface enhanced Raman scattering (SERS) measurements on the isolated chromophore and on EGFP and E^2GFP [5]. Without entering now into the details of classification of the vibrational modes, we just mention that it is possible to identify and assign some fingerprint modes that distinguish EGFP from E^2GFP being peculiar of B and A state respectively.

The detailed analysis of how each interaction influences the excitation energy of the chromophore has been also an important guide to establish some requirements for the dark state responsible for switching off of E^2GFP. We performed measurements of the absorption spectrum of E^2GFP in solution before and after irradiation with 476-nm light (the wavelength at which photobleaching/off-switching is accomplished) [7]. From the differential absorption it clearly emerges that depopulation of the bright B state associates with increasing strength of a band around 360 nm, which we attribute to population of the dark state. By contrast, illumination with 350-nm light (which is responsible for switching the protein back to the on state) of the photobleached sample shows a decreasing band at 360 nm accompanied with repopulation of the B state. We were thereby able to spectrally characterize the dark state (C in the following) and also to give a rough estimate of the transition rates between the involved states. These rates can be traced back to the average number of absorbed photons needed to toggle a single E^2GFP protein to the off state ($\sim 10^7$) and from the off state back to the on state ($\sim 10^6$). These values agree with measurements on clusters of E^2GFP molecules trapped in polyacrylamide gel (Fig. 2). Such measurements were performed with various irradiation intensities, and the irradiation times needed for efficient photoconversion were estimated. This is the first investigation of the dynamics of on and off switching. Having established that the C state absorbs at 360 nm (i.e. almost 40 nm blue-shifted with respect to the A state) and with the aid of the previously mentioned quantum mechanics calculations we were able to conclude that such state contained a neutral chromophore in a less coordinated environment, i.e. with less hydrogen bonds than in the normal configuration of state A [8].

An intriguing mechanism to explain the photoconversion of E^2GFP is cis-trans photoisomerization of the chromophore. These processes are responsible for non radiative relaxation from the excited state and take place thanks to intersections between the ground-state and excited-state potential-energy surfaces. However, the cis and the trans isomers of the chromophore have very similar excitation energies [9], so that the blue shift following photoconversion does not seem compatible with cis-trans isomerization. Interestingly, by performing a molecular dynamics simulation of the cis-trans photoisomerization process, we observed that the presence of a trans chromophore in the protein forces a configuration in which -at least- one hydrogen bond between the chromophore and the environment is absent. Thus, the protein containing a trans chromophore meets the structural requirements for blue-shifted excitation energy [8].

References

[1] R. J. Tsien, Annu. Rev. Biochem. **67**, 509 (1998); Z. Zimmer, Chem. Rev. **102**, 759 (2002); V. Tozzini, V. Pellegrini, and F. Beltram, in *Handbook of organic photochemistry and photobiology*, Chapter 139, edited by W. M. Horsphool and F. Lenci, CRC Press/Lewis Publisher (2003).

[2] R. M. Dickson, A. B. Cubitt, R. Y. Tsien, and W. E. Moerner, Nature **388**, 355 (1997).

[3] R. A. G. Cinelli, V. Pellegrini, A. Ferrari, P. Faraci, R. Nifosì, M. Tyagi, M. Giacca, and F. Beltram, Appl. Phys. Lett. **79**, 3353 (2001).

[4] R. Nifosì and V. Tozzini, Proteins **51**, 378 (2003).

[5] V. Tozzini, A. R. Bizzarri, V. Pellegrini, R. Nifosì, P. Giannozzi, A. Iuliano, S. Cannistraro, and F. Beltram, Chem. Phys. **287**, 33-42 (2003).

[6] T. Laino, R. Nifosì, and V. Tozzini, to be published in Chem. Phys.

[7] A. F. Bell, X. He, R. M .Wachter, and P. J. Tonge, Biochemistry **39**, 4423 (2000).

[8] R. Nifosì, A. Ferrari, C. Arcangeli, V, Tozzini, V. Pellegrini, and F. Beltram, J. Phys. Chem. **107**, 1679 (2003).

[9] W. Weber, V. Helms, J. A. McCammon, and P. W. Langhoff, Proc. Natl. Acad. Sci. USA **96**, 6177 (1999).

INTER EDGE-STATE TUNNELING IN THE FRACTIONAL QUANTUM HALL REGIME

Stefano Roddaro, Vittorio Pellegrini, Fabio Beltram, Giorgio Biasiol, Lucia Sorba, Roberto D'Agosta, Roberto Raimondi, Giovanni Vignale

A two dimensional electron gas (2DEG) in the fractional quantum Hall (FQH) regime shows a host of "exotic" phenomena driven by electron-electron interactions [1]. The fundamental charged excitations of FQH liquids are predicted to display fractional charges [2] and to obey fractional statistics. In addition, the one-dimensional (1D) edge states flowing at the boundary of incompressible FQH phases can form not-Fermionic chiral Luttinger liquids (χLL), as first predicted by Wen [3].

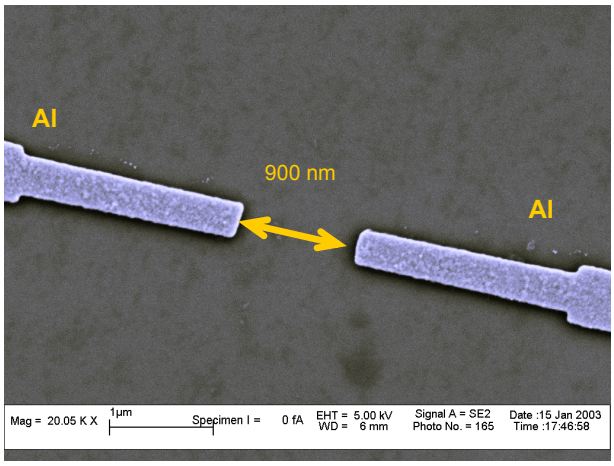

Figure 1 SEM picture of one of the devices fabricated at NEST. Constrictions consist of Al split-gates fabricated on GaAs/AlGaAs samples by e-beam lithography. Biasing the split-gate it is possible to deplete the portions of the 2DEG in the vicinity of the metallic gates. Further biasing can be exploited to finely tune the constriction.

Recent advances in nano-fabrication and experimental techniques opened the way to a deeper understanding of FQH liquids. Quantum point contacts (QPCs), for instance, can be used to induce controllable inter-edge scattering and were exploited to measure line-shapes in resonant inter-edge tunneling [4] or to infer the charge of the quasi-particles in shot noise measurements [5]. Antidot configurations were also nanofabricated to investigate quasi-particle transport [6]. Alternative fabrication techniques, such as cleaved-edge overgrowth, allowed the test of Luttinger- to Fermi-liquid tunneling characteristics [7]. In turn, these experimental findings stimulate new theoretical efforts aimed at unraveling the properties of collective excitations in these low-dimensional systems.

Tunneling between edge states in the FQH regime is deeply affected by many-body effects. For this reason a careful analysis of the tunneling characteristics can provide very valuable information to test theoretical models for FQH systems. In a real device, a controllable inter-edge tunneling of electrons or fractionally-charged quasi-particles in a FQH state can be obtained at a QPC depending on the constriction parameters. In the *weak-backscattering* limit the quantum Hall fluid is weakly perturbed by the QPC constriction. In this case the inter-edge current (at filling factor $\nu = 1/q$, where q in an odd integer) consists of fractional quasi-particles of charge e*=νe that back-scatter between the edges through the quantum Hall fluid. At T = 0 the quasi-particles tunneling rate is predicted [3,8] to grow at low voltages as $I_T \sim V_T^{2\nu-1}$. At finite temperature, below a critical value $V_{T,max} \sim K_B T/e^*$, the tunneling current reverts to the linear behavior. This leads to a differential tunneling characteristics (dI_T/dV_T) showing a peak centered at $V_T=0$ with a width $\Delta V_T \sim V_{T,max}$. It is particularly interesting to investigate this tunneling regime: a detailed analysis of the conductance characteristics can yield a direct measurement of the effective charge e* involved in the tunneling process. By a suitable biasing of the split-gate it is also possible to induce a strong coupling between the edge states and address the *strong-backscattering* limit. The transition from the *weak-* to the *strong-backscattering* regime represents an additional challenging issue [9] and can be driven by changes in temperature, inter-edge voltage drop and QPC configuration.

This work focused on the fabrication and ultra-low-temperature measurement of constrictions on low-density (less than 1×10^{11} cm^{-2}) and high-mobility (1×10^{6} cm^2/Vs) GaAs/AlGaAs heterostructures. Samples were grown at the NEST molecular beam epitaxy facility located at the TASC-INFM

laboratory in Trieste, while processing and measurement of devices were preformed in Pisa. This work was done in close collaboration with theoretical groups (NEST groups at University of Roma III, University of Missouri-Columbia). During this work we explored different fabrication techniques and geometries for QPCs and final devices were processed by Al split-gating as this technique was the most suitable for our experiments. Figure 1 reports a scanning electron microscope (SEM) picture of one of the devices fabricated in Pisa. Constrictions in a strong magnetic field can induce a controllable backscattering between opposite-flowing edge states (see Fig. 2). Four-wire measurements (R_{xx}) across the constriction directly yield the backscattering rate, which is in turn related to the inter-edge tunneling amplitude. Indeed it can be shown that, when the bulk 2DEG is insulating (i.e. in the quantum Hall regime), the following relation holds

$$R_{xx} = \rho_{xy}^2 \frac{dI_T}{dV_T} \,. \qquad (1)$$

By applying a finite DC current bias I to the Hall bar (see Fig. 2), a transverse Hall voltage V_H can be induced. That voltage corresponds to the potential difference between edges, i.e. $V_T=\rho_{xy}I$. By tuning the DC current I it is possible to directly measure the dI_T/dV_T vs. V_T curve.

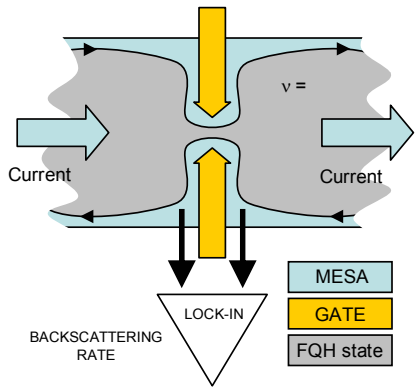

Figure 2 Inter-edge tunneling at a constriction: the split-gate in the center induces a controllable backscattering that can be detected differentially by a phase-locked four wire measurement. The blue region indicates the Hall bar, while the grey area represents an incompressible FQH state at $\nu=1/3$. A finite DC current bias I is used to control the inter-edge tunneling bias (Hall voltage) $V_T=\rho_{xy}I$. Backscattering rate is directly related to tunneling conductance through $R_{xx}=\rho_{xy}^2 dI_T/dV_T$.

Figure 3 reports a set of tunneling data at a QPC constriction fabricated starting from a single heterojunction located 100 nm below the surface with mobility $\mu \sim 1.0\times10^6$ cm^2/Vs and charge density $n \sim 0.6\times10^{11}$ cm^{-2}. Devices were patterned with rectangular split-gates (width was 600 nm, length was 300 nm). Data refer to different temperatures ranging from 30 mK to 900 mK. We observed a conductance peak for $T \geq 300$ mK which is qualitatively compatible with Wen's theory. Unexpectedly, while theory predicts a sharpening of the peak for lower temperatures, experimental curves display a deep minimum for $T < 300$ mK. This behavior is unexplained at present. We analyzed the experimental curves at higher temperatures following Wen's theory as well as a modification of it including the effects of inter-edge coulomb repulsion [10]. The fitted value for e*/e was greater than the expected 1/3 (~0.4 for Wen's theory, ~0.5 for the modified theory). We think this discrepancy could be related to the relatively high temperatures at which the peak appears: theory always considers single particle tunneling events while in this temperature regime many thermally activated quasi-particles populate the FQH liquid.

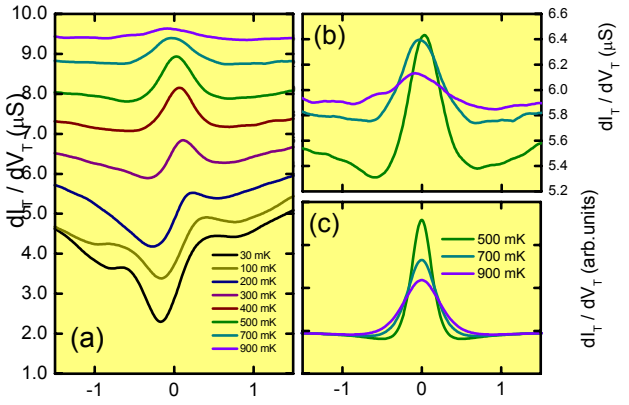

Figure 3 (a) Tunneling measurements at different temperatures. Data were shifted vertically for a better reading. In the high-temperature region a conductance peak at $V_T^{(b)}=0$, compatible with Wen's theory, was observed. For lower temperatures a different behavior shows up and a sharp, still unexplained, minimum develops. Experimental data in the high temperature regime **(b)** are qualitatively consistent with Wen's theory **(c)**.

We plan to continue this research activity with the fabrication of more complex devices addressing specific properties of the FQH states. In particular we plan to process constrictions connecting two-dimensional regions at different filling factors [12] (1 and 1/3 in the most simple case) as well as an inter-edge Fabry-Perot interferometer [13]. The first device addresses the problem of the injection of electrons into a FQH edges through an Andreev-like scattering. The second device can be used to demonstrate the fractional statistics of the quasi-particles in the FQH regime.

References:

[1] T. Chakarborty and P. Pietilainen in *The Quantum Hall Effects: Fractional and Integral*, Springer-Verlag (1995).
[2] R. B. Laughlin, Phys. Rev. Lett. **50**, 1395 (1983).
[3] X. G. Wen, Phys. Rev. Lett. **64**, 2206 (1990); Phys. Rev. B **41**, 12838 (1991); Phys. Rev. B **43**, 11025 (1991), Phys. Rev. B **44**, 5708 (1991).
[4] F. P. Milliken *et al.*, Solid State Commun. **97**, 309 (1995).
[5] D. C. Glattli *et al.*, Physica (Amsterdam) **6E**, 22 (2000). R. De Picciotto *et al.*, Nature **389**, 162 (1997); L. Saminadayar *et al.*, Phys. Rev. Lett. **79**, 2526 (1997); T. G. Griffiths *et al.*, Phys. Rev. Lett. **85**, 3918 (2000); E. Comforti *et al.*, Nature **416**, 515 (2002).
[6] I. J. Maasilta and V. J. Goldman, Phys. Rev. B **55**, 4081 (1997).
[7] M. Hilke *et al.*, Phys. Rev. Lett. **87**, 186806 (2001); A. M. Chang *et al.*, Phys. Rev. Lett. **77**, 2538 (1996); M. Grayson *et al.*, Phys. Rev. Lett. **80**, 1062 (1998).
[8] C. L. Kane and M. P. A. Fisher, in *Perspectives in Quantum Hall Effects*, edited by S. Das Sarma and A. Pinczuk, Wiley, New York (1996).
[9] P. Fendley, A. W. W. Ludwig, and H. Saleur, Phys. Rev. Lett. **75**, 2196 (1995).
[10] R. D'Agosta, R. Raimondi, and G. Vignale, Phys. Rev. B, in press.
[11] S. Roddaro, V. Pellegrini, F. Beltram, G. Biasiol, L. Sorba, R. Raimondi, and G. Vignale, Phys. Rev. Lett. **90**, 046805 (2003).
[12] D. B. Chklovskii and B. I. Halperin, Phys. Rev. B **57**, 3781 (1998).
[13] C. de C. Chamon, D. E. Freed, S. A. Kivelson, S. L. Sondhi, and X. G. Wen, Phys. Rev. B **55**, 2331 (1997).

CLASSICAL INFORMATION TRANSFER OVER NOISY QUANTUM CHANNELS WITH MEMORY

G. Massimo Palma, Chiara Macchiavello

Entanglement is now regarded as one of the key ingredients - if not the key ingredient - of all the known quantum information processing algorithms and protocols. In most cases the information which is processed more efficiently with a supply of entanglement is of quantum nature, like e.g. in the case of teleportation. However we have shown that entanglement is a useful resource also in the transmission of classical information, i.e. entanglement plays a role in the context of the classical capacity of some quantum channels. The classical capacity of a quantum channel [1] is, roughly speaking, the amount of classical information that can be reliably transmitted by using quantum states in the presence of a noisy environment. Its study has attracted much interest recently. One of the main objects of such an interest is indeed the role played by entanglement: if we encode the information into quantum states there may be the possibility that by entangling multiple uses of the channel a larger amount of classical information per use can be reliably transmitted. This property is known as superadditivity. Attention so far has been paid to memoryless channels, i.e. to channels in which independent noise acts on each use. The absence of superadditivity was first proved analytically for the case of two entangled uses of the depolarising channel [2] and then extended to a broader class of memoryless channels. However it has been later shown [3] that entanglement is a precious resource to increase the information transmission when the noise introduced by the channel exhibits some correlations among subsequent uses.

We have assumed that each use of the channel will be a qubit, i.e a quantum state belonging to a two-dimensional Hilbert space. In the simplest scenario the transmitter can send one qubit at a time through the channel. In this case the message to be transmitted is encoded in codewords that are tensor products of the states of the individual qubits. Quantum mechanics however allows also the possibility to entangle multiple uses of the channel, and thus to encode the classical information to be transmitted into entangled states.

The maximum mutual information of a general quantum channel $\$$ is given by the Holevo-Schumacher-Westmoreland bound [1]

$$I = Max_{\{pi,\ \rho i\}}\ S(\ \$(p_i\rho_i)) - \Sigma_i\_p_i S(\$(\rho_i))$$

where $S(\omega) = - Tr\ \omega \log \omega$ is the von Neumann entropy of the density operator ω and the maximization is performed over all input ensembles $\{p_i,\ \rho_i\}$ into the channel. Note that such bound includes a maximization over the POV measurement, also collective ones, at the receiver.

A channels is generally described in terms of Kraus operators [5] A_i satisfying $\Sigma_i A^+_i A_i = I$ such that if we send through the channel a qubit in a state described by the density operator ρ the corresponding output state of the channel is given by the map $\$(\ \rho) = \Sigma_i A_i\ \rho\ A^+_i$

The depolarizing channel is a channel whose actions are proportional either to the identity or to the three Pauli operators σ_2 (this latter with equal weight). Such actions describe isotropic noise and lead to a shrinking of the Bloch vector of the input qubits.

A memoryless quantum channels is a channels whose action on arbitrary input states consisting of n qubits (including entangled ones) can be written as tensor product of n Kraus operators acting on each individual input qubit.

For the memoryless depolarizing channel it has been shown the mutual information is maximized by any set of orthogonal product states, and therefore the use of entangle signal states is not beneficial.

Things are different in the case in which the channel is characterized by a certain degree of memory. The actions of the depolarising channel with memory, for the case of two qubits take the following form:

$$A_{1,2} = \{\ p_1[(1- \mu)\ p_2 + \mu\ \delta_{k2,k1}\}^{1/2}\ \sigma_{k1}\ \sigma_{k2}$$

This means that with probability μ the same action is applied to both qubits while with probability $1 - \mu$ the two actions are uncorrelated. The parameter μ describes the degree of memory of the channel. From the physical point of view, this noise model can describe situations where time

correlations are present in the system. For instance, μ could depend on the time lapse between the two channel uses. If the two qubits are sent at a very short time interval one after the other, the properties of the channel, which determine the direction of the random noise, will be unchanged and it is therefore reasonable to assume $\mu = 1$. If on the other hand, the time interval between the channel uses is such that the channel properties have changed then the channel is memoryless and $\mu = 0$.
It is immediate to verify that for the case of perfect memory the maximally entangled Bell states are eigenstates of the noise operators and therefore will pass undisturbed through the channel. If used as equiprobable signal states they maximize the mutual information. Furthermore it is immediate to verify that the I will assume a smaller value by any ensemble of tensor product input states. This situation is reminiscent of the so called noiseless codes, where collective states are used to encode and protect quantum information against collective noise [6].
In general we have shown that in the presence of collective noise the transmission of classical information can be enhanced by employing maximally entangled states as carriers of information instead of product states. In particular, for channels with correlated noise our results show that a higher mutual information can indeed be achieved above a certain memory threshold, which depends on the characteristics of the channel, by entangling two consecutive uses of the channel. This result broadens the class of situations in which the use of entanglement enhances the efficiency in communications and information processing.
Work is in progress to understand whether the onset of the threshold value in the degree of memory can be identified for a more general class of quantum transmission channels.

Collaborations
This activity is carried out in collaboration with Università di Pavia.

References
[1] B. Schumacher and M. D. Westmoreland, Phys. Rev. A **56**, 131 (1997); A. S. Holevo, IEEE Trans. Inf. Theory **44**, 269 (1998) (also quant-ph/9611023);
[2] D. Bruss, L. Faoro, C. Macchiavello and G. M. Palma, J. Mod. Opt. **47**, 325, 2000; (also quant-ph/9903033).
[3] C. King, quant-ph/0103156; C. King, quant-ph/0204172.
[4] C. Macchiavello and G. M. Palma, Phys. Rev. A **65**, R050301 (2002).
[5] M. Nielsen and I. Chuang, *Quantum computation and quantum information*, Cambridge University Press (2000); A. Peres *Quantum Theory: concepts and methods*, Kluwer Academic Publishers, (1995).
[6] G. M. Palma, K.-A. Suominen and A. K. Ekert, Proc. Roy. Soc. London A **452**,567 (1996); for a recent review see J. Kempe, D. Bacon, D. A. Lidar, K. B. Whaley. Phys. Rev. A **63**, 2307 (2001).

THEORY OF SUPERCONDUCTOR NANOSTRUCTURES

Alessandro Romito, Rosario Fazio, Francesco Plastina

A well studied example of physical processes where electron correlations play a dominant role is the phenomenon of Coulomb blockade. In a system of small tunneling junctions, due to the large electrostatic energy (as compared to temperature or voltages), the electronic charge is transported one by one. This effect leads to many remarkable features in transport properties and has been a subject of extensive study for the last decades. As an example, the strong dependence of the current-voltage characteristics on the gate charge was exploited to use a single electron transistor (SET) as a highly sensitive charge detector, and proposed as measuring apparatus of the charge state of a Josephson quantum bit. Since it leads to a strong correlation of consecutive tunneling events, Coulomb blockade has turned out to manifest itself in a peculiar way on the average current and on electrical noise.
In this paper, we analyze a superconducting double tunnel junction device, operating in a suitably chosen bias voltage regime, such that one of the junctions of the SET is on resonance for Cooper pair tunneling. The interplay between coherence and interaction is explored by sweeping the operating point of the device through the Cooper pair resonance. We will show that the fluctuations of the charge on the central island are sensitive to both Coulomb blockade and quantum coherence. More pronounced effects arise in the regime in which the rates of incoherent quasi-particle tunneling matches the frequency of coherent Cooper-pair oscillation. This gives rise to an enhanced fluctuation of charge in the central-island and to a substantial suppression of the current noise. By investigating the statistics of the tunneling events, we show that the suppression in the shot noise is related to the deviation of the counting statistics from the Poissonian distribution. The probability distribution of tunneling events exhibits a parity dependence and remains non-Poissonian in a wide range of parameter values. The interplay between coherence and Coulomb blockade affects the overall charge transport and is also clearly observed in the finite frequency behavior of the current noise. Its power spectrum displays a sharp resonance peak at the Josephson frequency, resulting from coherent oscillations between two quantum states.
In the figures shown below typical behavior of noise power spectrum S(ω) as a function of frequency ω. The various curves are obtained for different values of the resonance frequency.

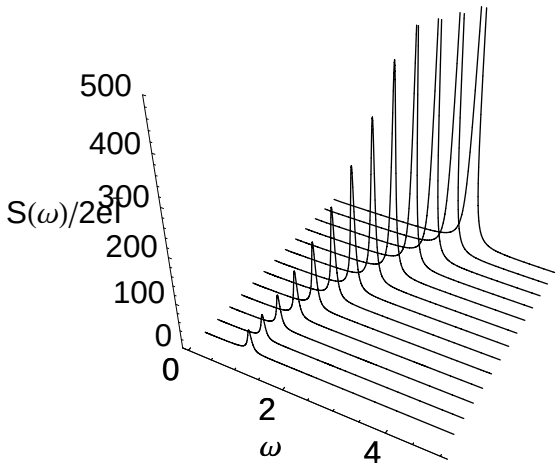

Figure 1

Quite recently it was realized that superconducting SET transistors could be also implemented using nanomechanical resonators. In this case, then, the physics of Coulomb blockade could be fruitfully combined in devices with mechanical part. Very recently, Gorelik *et al.* proposed a very appealing setup, named Cooper pair shuttle, able to create and maintain phase coherence between two distant

superconductors. In its simplest realization the system consists of a superconducting grain periodically moving between two superconducting electrodes. Despite the fact that the grain is in contact with only one lead at a time, this shuttle not only carries charge, as in the not superconducting case, but it also establishes phase coherence between the leads. We analyzed how an external environment affects the coherent transport in the Cooper pair shuttle. The interplay between the driving (mimicked by the motion of the grain) and the environmental dephasing leads to several interesting results. We showed, for example, that increasing the coupling to the environment may result in an *enhancement* of the supercurrent as well as in a change of its sign π-junction. We also proposed an implementation of the shuttle, based on the controlled switching of an external magnetic field, that does not require any moving grain. In this way it is possible to control the effect of the environment, and to check the predictions of this work, by changing the time dependence of the applied field.

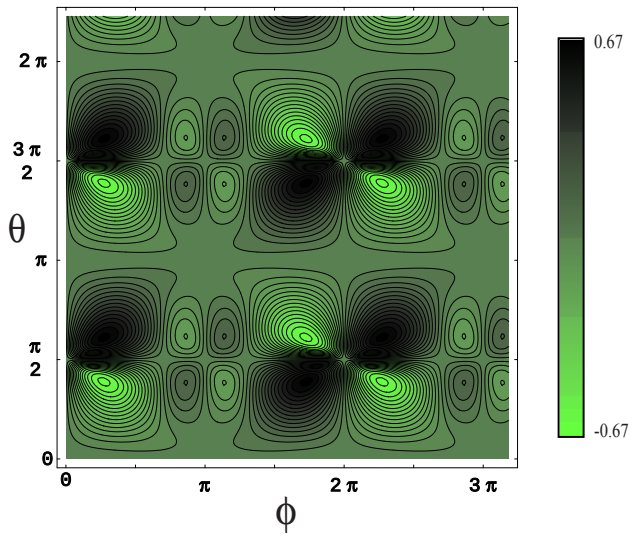

Figure 2

The picture above is a contour plot of the supercurrent as a function of the phase difference and of the dynamical phase accumulated due to the Josephson coupling. It is more evident in the next figure the fact that the current can even increase on increasing the damping γ.

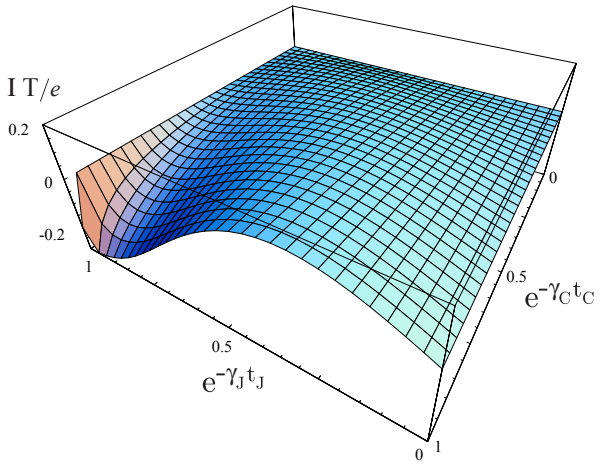

Figure 3

References

[1] M.-S. Choi, F. Plastina, and R. Fazio, Phys. Rev. Lett. **87**, 116601 (2001) & Phys. Rev. B **67**, 045105 (2003).

[2] A. Romito, F. Plastina, and R. Fazio *Decoherence in the Cooper pair shuttle*, Phys. Rev. B **68**, 140502R (2003).

SOLID STATE QUANTUM COMPUTATION

Luigi Amico, Rosario Fazio

In recent years it has become clear that the laws of quantum mechanics allow for exponentially more efficient ways of performing computation. The origin of such exponential efficiency can be ascribed to the intrinsic parallelism of quantum time evolution and can be understood by viewing quantum computers as programmable quantum interferometers. In this description a quantum computer, initially prepared in a superposition of all its input states, evolves in parallel along all the various computational paths, which will interfere constructively towards the desired output state. The design of any quantum computing device therefore must give prescriptions on how to prepare superposition of states of a suitable physical system, how to introduce the desired phase difference among the various possible computational paths and how to measure the output state.
The quest for large scale integrability and flexibility in the design of quantum computing devices has very recently stimulated an increasing interest in the field of solid state physics. The natural arena to implement quantum information protocols is that of nanostructures. Up to now several different systems have been proposed both in the field of semiconducting and superconducting materials.
Josephson junctions have recently attracted much attention as candidate physical systems for the technological implementation of quantum computation. Much of their appeal comes from the interest for systems amenable of large scale integration. Furthermore astonishing progress has recently been made in the control of their coherent evolution.
Among the various proposed schemes, the activity within NEST concentrated on the proposal where the information is encoded in the charge state of a small superconducting electron boxes. The system consists of two small superconducting islands coupled by a tunnel junction with Josephson energy E_J and capacitance C_J. The electrostatic energy of the island can be controlled by a capacitive coupling (of capacitance C) to an external bias voltage V. For small capacitance C_J the electrostatic energy limits the number of Cooper pairs on the island. In this setup a suitable basis to encode our qubit consists of two charge states differing by one Cooper pair.
One of the greatest advantages of superconducting nanodevices is their flexibility in design. Recently it was shown that it is possible, already now, to implement simple algorithms. In the figure below

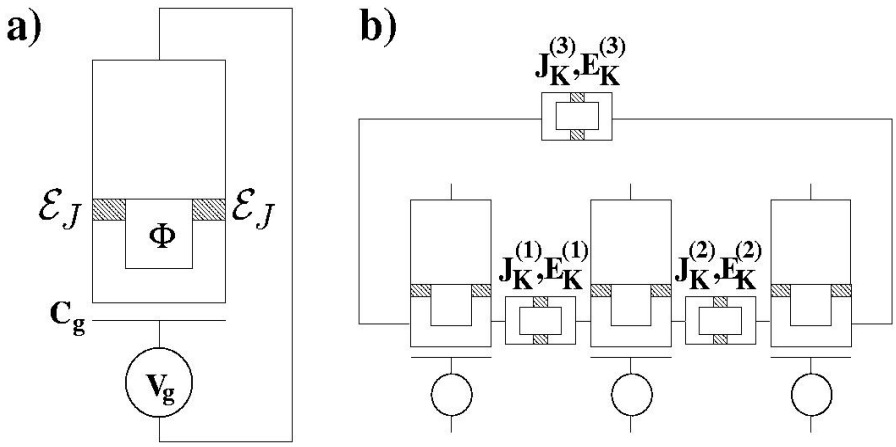

Figure 1

the circuit needed for the Deusch algorithm.
In most of the implementations proposed so far quantum computation is obtained by varying in time in a controlled way the Hamiltonian of the individual qubits as well as their mutual coupling. For instance the qubits are subject to external pulses or suitable qubit-qubit interaction are suddenly switched on and off. In all these cases the qubit phases are of a dynamical nature.
An alternative design makes use of quantum geometric phases, obtained by adiabatically varying the Hamiltonian in such a way to describe a suitably chosen closed loop in its parameter space.

It should be noted that the conventional theory of detection of Geometric phases is usually phrased exactly in the same interferometric terms as the one used above in connection with quantum computation. Recently it has been demonstrated by some of the researchers of NEST that geometric phases can be generated in a system of small coupled Josephson junctions and used to implement one and two qubit gate operations. The setup which was considered consists of a superconducting electron box formed by an *asymmetric* SQUID, pierced by a magnetic flux and with an applied gate voltage. As in the case of charge qubit, the device operates in the charging regime.

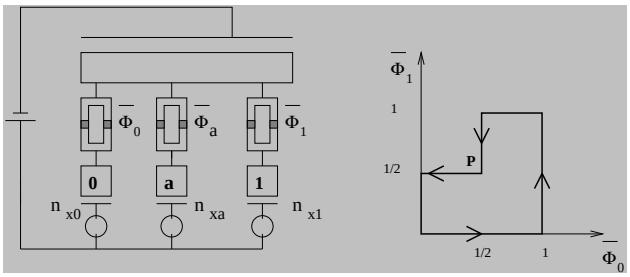

Figure 2

Understanding the properties of entanglement in solid state devices is currently under the scrutiny of the scientific community since it may be of great relevance both for proposing new schemes for implementing a quantum computer and for a deeper understanding of many body systems. A number of interesting results in this direction have already been obtained in the case of models of interacting spins. We recently focused our attention to the problem of entanglement close to a quantum phase transition. We showed that entanglement can been classified in the framework of scaling theory of phase transitions, however it has been demonstrated that there is a profound difference between non-local quantum and classical correlations. In the next plot we present one of the most central results of our work. The variation of entanglement shared by two neighboring spins as a function of the parameter λ which allows to sweep through the phase transition. The divergence at the critical point clearly shows changes occurring in the ground state wavefunction at the critical point.

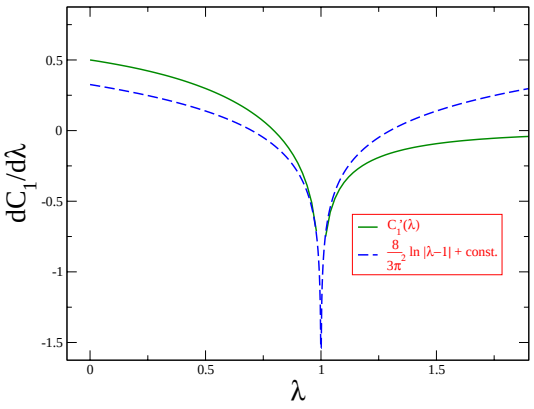

Figure 3

References

[1] J. Siewert and R. Fazio, Phys. Rev. Lett. **87**, 257905 (2001).
[2] L. Faoro, J. Siewert, R. Fazio, Phys. Rev. Lett. **90**, 028301 (2003).
[3] A. Osterloh. L. Amico, G. Falci, and R. Fazio, Nature **416**, 608 (2002).

CORRELATIONS IN LOW-DIMENSIONAL ELECTRONIC SYSTEMS

Reza Asgari, Francesco Capurro, Bahman Davoudi, Marco Polini, Mario P. Tosi

Many of the electron-electron interaction effects in simple metals and semiconductors can be understood by reference to the homogeneous electron-gas model. A central role is played by the electron-pair distribution functions $g^{\sigma\sigma'}(r)$, which describe how short-range exchange and correlations enter to determine the probability of finding two electrons with spin σ and σ' at a relative distance *r*. A precise definition of $g^{\sigma\sigma'}(r)$ is through the average number of electrons of spin σ contained in a spherical shell of radius *r* and thickness *dr* centered on an electron at the origin with spin σ', which is given by $n^{\sigma}g^{\sigma\sigma}(r)\Omega_D r^{D-1}dr$ where *D* is the space dimensionality, n^{σ} is the density of electrons with spin σ, and Ω_D the solid angle in *D* dimensions (with $\Omega_2=2\pi$ and $\Omega_3=4\pi$). The spin-average distribution function *g(r)* reflects the charge-charge correlations in the electron gas.

The mean potential energy of the unpolarized electron gas can be calculated from $g(r)=[g^{\uparrow\downarrow}(r)+g^{\uparrow\uparrow}(r)]/2$ and hence, through an integration over its dependence on the coupling strength, the total energy as well. Thus, an accurate knowledge of this function is crucial for applications of density functional theory (DFT) in various schemes that have been proposed to transcend the local density approximation (LDA) in the construction of exchange and correlation energy functionals.

Early calculations of the pair distribution functions in the *3D* electron gas were based on the use of a Bijl-Jastrow correlated wave function [1] for the ground state and on exploiting the fluctuation-dissipation theorem for a self-consistent determination from the charge and spin response functions [2]. These early results were validated with the advent of the Quantum Monte Carlo (QMC) techniques, which have produced a wealth of accurate data on correlation and response functions over a wide range

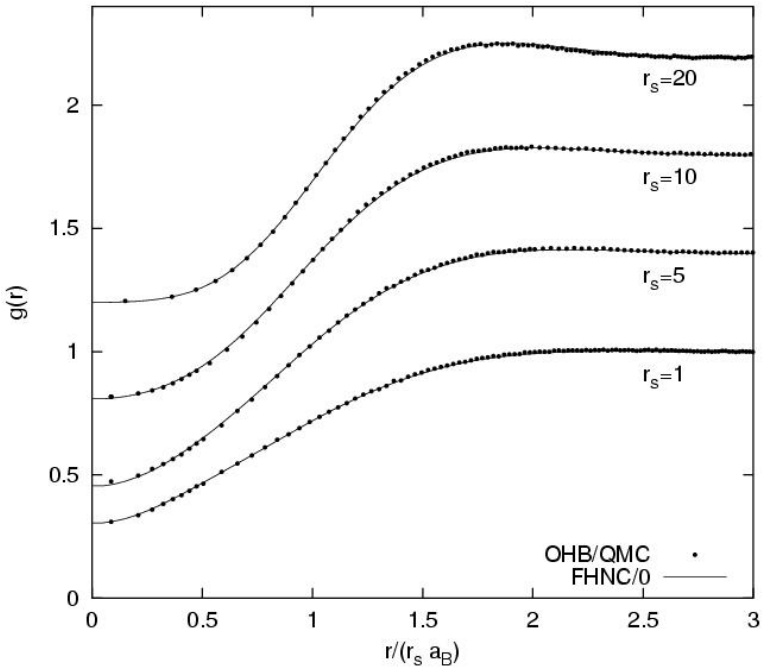

Figure 1 The pair distribution function *g*(*r*) in a paramagnetic *3D* EG at r_s=*1,5,10* and *20*, as a function of $r/(r_s a_B)$. The results of FHNC/0 approximation [11] (full lines) are compared with QMC data of Ortiz *et al.*[4] (dots). The curves at r_s=*1,5,10* and *20* have been shifted upwards for clarity by *0.4, 0.8* and *1.2*, respectively.

of coupling strength for both the *3D* [3,4] and the *2D* case [5]. The QMC data have in turn stimulated a number of further theoretical studies.
In a seminal work Overhauser [6] developed a wholly different approach to the evaluation of $g^{\uparrow\downarrow}(0)$ in *3D* jellium, in which he tackled the electron-electron scattering problem in the many-body system through the solution of an effective Schrödinger equation for the relative motion of an electronic pair. The approach of Overhauser has subsequently been used to evaluate $g^{\uparrow\downarrow}(0)$ in the *2D* electron gas, and has been extended by Gori-Giorgi and Perdew [7] to evaluate $g(r)$ at finite r in *3D* through an accurate numerical solution of Overhauser's two-body Schrödinger equation.

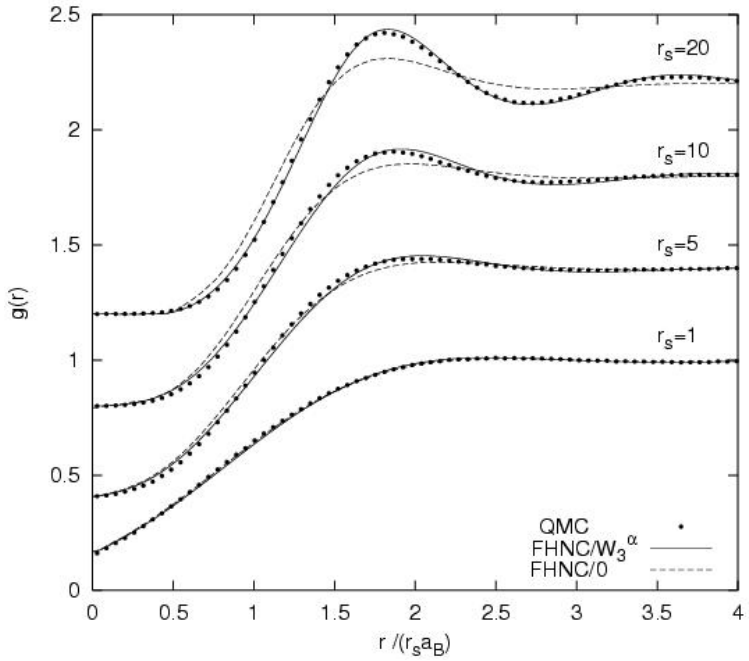

Figure 2 The pair correlation function of a *2D* paramagnetic electron gas as a function of $r/(r_s a_B)$ at r_s=*1,5,10* and *20*. We present the results of the FHNC/0 (dashed line) approximation and FHNC/ W_3^{σ} approximation [12] (solid line) and compare them with the QMC results [13] (dots). The curves at r_s=*1,5,10* and *20* have been shifted upwards for clarity by *0.4, 0.8* and *1.2*, respectively.

We have further developed this approach to the evaluation of the pair distribution functions by adopting a self-consistent Hartree scheme for the determination of the effective potential entering the two-body Schrödinger equation, carrying out calculations for both a *3D* and a *2D* electron gas [8]. This approach proved to give excellent agreement with QMC data in the intermediate coupling regime in both *3D* and *2D*. On increasing the coupling strength the pair distribution function from the QMC work starts developing a first-neighbor peak, and this behavior is not reproduced quantitatively by the theory. As may be expected, the Hartree approximation is quantitatively useful in *2D* over a more limited range of coupling strength and has more limited accuracy in regard to the splitting of the exchange-correlation hole into its parallel- and antiparallel-spin components. We have also examined [9] whether the inclusion of exchange and correlation in the electron-electron effective interactions as derived by Kukkonen and Overhauser [10] allows one to transcend the results yielded by the Hartree approximation on *2D* jellium in the strong coupling regime.
In a recent paper [11] we formulate an analytic theory for spin correlations in the spin-polarized *3D* EG. The fluid that we consider consists of two spin components at fixed average densities n^{σ} with $\sigma = \uparrow$ or $\downarrow$, and the spin correlations are described by the pair distribution functions $g^{\sigma\sigma'}(r)$. The general strategy is to set up a Schrödinger-like differential equation for $\sqrt{g}^{\sigma\sigma'}(r)$ with the help of the Hohenberg-Kohn variational principle and to solve it by a Fermi-hypernetted-chain type of approximation (FHNC/0) tailored to embody the Hartree-Fock limit as well as a set of sum rules for the two-component Fermi fluid. The numerical results given by this approximation are in very good agreement with QMC data in the weak and intermediate coupling strength region (Fig. 1), although they fail to produce the pair correlation function with the same quality in the high coupling strength

limit or in low dimensional systems. We think that the source of the problem in FHNC/0 approximation is in the *bosonic* part of the effective potential.
In our last work [12] we introduce a model for an effective potential to improve the one which enters the Fermi hypernetted chain equations. Our study is limited to the *2D* system in which the correlation effects are stronger and most of the approximations fail to give good results for the pair correlation function even in the intermediate coupling region.
We show explicitly with our numerical results that once we produce a good effective potential for a Bose system, we can use this potential as the bosonic part of the effective potential for a Fermi system. Our strategy is to add the contribution of the three body correlation functions in the effective potential of the Bose system which contains an extra free parameter (HNC/W_3^{σ}). We fix the parameter such that the correlation energy given by this model equals the QMC correlation energy of the same Bose system [14]. With this potential in our disposal, we can find the contribution of the three body correlation in the effective potential for the Fermi system (FHNC/ W_3^{σ}).

In conclusion we find a model for the effective potential which permits us to get the pair correlation function in excellent agreement with the Monte-Carlo computational results in the whole range of the density (Fig. 2). We have therefore achieved full understanding of the physical factors that determine instantaneous pair correlations in degenerate quantum plasmas.

References:

[1] L. J. Lantto and P. J. Siemens, Nucl. Phys. A **317**, 55 (1979); L. J. Lantto Phys. Rev. B **22**, 1380 (1980).
[2] K. S. Singwi, M. P. Tosi, R. H. Land, and A. Sjölander, Phys. Rev. **176**, 589 (1968); R. Lobo, K. S. Singwi, and M. P. Tosi, ibid. **186**, 470 (1969).
[3] D. M. Ceperley and B. J. Alder, Phys. Rev. Lett. **45**, 566 (1980); B. J. Alder, D. M. Ceperley, and E. L. Pollock, Int. J. Quant. Chem. **16** 49 (1982).
[4] G. Ortiz and P. Ballone, Phys. Rev. B **50**, 1391 (1994) and **56**, 9970 (1997); G. Ortiz, M. Harris, and P. Ballone, Phys. Rev. Lett. **82**, 5317 (1999); P. Gori-Giorgi, F. Sacchetti, and G. B. Bachelet, Phys. Rev. B **61**, 7353 (2000).
[5] B. Tanatar and D. M. Ceperley, Phys. Rev. B **39**, 5005 (1989); S. Moroni, D. M. Ceperley, and G. Senatore, Phys. Rev. Lett. **69**, 1837 (1992); F. Rapisarda and G. Senatore, Austr. J. Phys. **49**, 161 (1996); D. Varsano, S. Moroni, and G. Senatore, Europhys. Lett. **53**, 348 (2001); C. Attaccalite, S. Moroni, P. Gori-Giorgi, and G. Bachelet, Phys. Rev. Lett. **88**, 256601 (2002).
[6] A. W. Overhauser, Can. J. Phys. **73**, 683 (1995), R. Asgari, M. Polini, B. Davoudi, and M. P. Tosi, Solid State Commun. **125**, 139 (2003).
[7] P. Gori-Giorgi and J. P. Perdew, Phys. Rev. B **64**, 155102 (2001).
[8] B. Davoudi, M. Polini, R. Asgari, and M. P. Tosi, Phys. Rev. B **66**, 075110 (2002).
[9] F. Capurro, R. Asgari, B. Davoudi, M. Polini, and M. P. Tosi, Z. Naturforsch. **57 a**, 237 (2002).
[10] C. A. Kukkonen and A. W. Overhauser, Phys. Rev. B **20**, 550 (1979).
[11] B. Davoudi, R. Asgari, M. Polini, and M. P. Tosi, cond-mat/0305281
[12] R. Asgari, B. Davoudi, and M. P. Tosi, in preparation.
[13] S. Moroni, private communication.
[14] S. De Palo, S. Conti, and S. Moroni, cond-mat/0306145

DYNAMICS OF TRAPPED TWO-COMPONENT FERMI GASES

Patrizia Vignolo, Federico Toschi, Sauro Succi, Mario P. Tosi

After the achievement of Bose-Einstein condensation [1] a main goal of experimentalists is to cool a Fermi gas down into the superfluid regime. The cooling process used is the evaporative one, where the most energetic particles are expelled from the trap and the others re-thermalize through collisions. However, at very low temperatures the main collisional processes occur in the *s*-wave channel, which is avoided by the Pauli principle for a spin-polarized Fermi gas. To circumvent this problem a bosonic component, or a second fermionic component polarized in another isospin-state [2] is added in the trap, but the fermionic gas can still be cooled only down to temperatures of *0.1-0.2* times the Fermi temperature T_F. This limit is due again to the Pauli principle. Let us focus on the two-component Fermi gas. In this case the collisional rate term $C_{12}[f^{(j)}]$ for the fermionic component j, described by the Wigner distribution $f^{(j)}(\mathbf{r},\mathbf{p},t)$, is proportional to the "classical" cross-section $\sigma=\pi a^2$ with a the mutual scattering length between the two components, weighted by the population factors of the initial and final states involved in the collision:

$$C_{12}[f^{(j)}] \propto \sigma \sum_{\mathbf{p}_2,\mathbf{p}_3,\mathbf{p}_4} \Delta_{\mathbf{p}} \Delta_{\varepsilon} \left[\bar{f}^{(j)} \bar{f}_2^{(\bar{j})} f_3^{(j)} f_4^{(\bar{j})} - f^{(j)} f_2^{(\bar{j})} \bar{f}_3^{(j)} \bar{f}_4^{(\bar{j})}\right]$$

with

$$f^{(j)} \equiv f^{(j)}(\mathbf{r},\mathbf{p},\mathbf{t}), \ \bar{f}^{(j)} \equiv 1 - f_i^{(j)}, \ f_i^{(j)} \equiv f^{(j)}(\mathbf{r},\mathbf{p}_\mathbf{i},t), \ \bar{f}_i^{(j)} \equiv 1 - f_i^{(j)}$$

The factors Δ_p and Δ_ε are the usual delta functions accounting for conservation of momentum and energy. On cooling all space-phase cells of volume h^3 become quasi-fully occupied and the collisional events are strongly suppressed by the populations factors (Pauli blocking). The fermions do not thermalize efficiently enough, causing failure of the evaporative cooling method.

An important tool to study the problem of Pauli blocking and design new set-ups is through numerical experiments. For this purpose, we have developed a numerical code to simulate the dynamics of a two-component Fermi gas in an axially-symmetric geometry. We solve the Vlasov-Landau Equations (VLE) for the Wigner distributions $f^{(j)}$ using a particle-in-cell method to describe the real-space particle distribution. Each fermion is represented by means of N_q computational particles ("quarks"). The i-th quark is located in momentum space by using Monte Carlo sampling and making sure that each cell of volume h^3 is occupied by no more than N_q quarks. In the propagation step the particles move under the action of external and mean-field forces through a Verlet algorithm. Each possible pair of quarks in each space-phase cell is evaluated.

As a first application we have studied [3] a mixture of ^{40}K atoms polarized in the *7/2* and *9/2* isospin states, for system parameters ranging from the collisionless to the hydrodynamic regime. The initial equilibrium density profiles are rigidly displaced from the center of the harmonic trap and start to oscillate. In the absence of interactions they would keep oscillating at their respective trap frequencies without damping. We switch on the interactions and vary the collision rate by changing the scattering length, thus mimicking the exploitation of a Feshbach resonance [4]. The transition from the collisionless to the collisional regime at various temperatures is shown both in the plot of the frequency of the dipole mode for the two components in Fig. 1(a) and in the plot of the damping rate $\gamma=1/\tau$ of the axial motion of the centers of mass $z^{(j)}_{cm}(t)$ in Fig. 2(b). At very low collision rate Γ_q the dipole mode frequencies are given by the corresponding trap frequencies with a shift due to the mean-field potential. At intermediate values of Γ_q the data points show large fluctuations, due to the fact that in this region just a few collisions can drastically alter the motion of the clouds. However, the trend towards a locking of the two dipole mode frequencies at large Γ_q is very clear and the location of the locking is identified with reasonable accuracy.

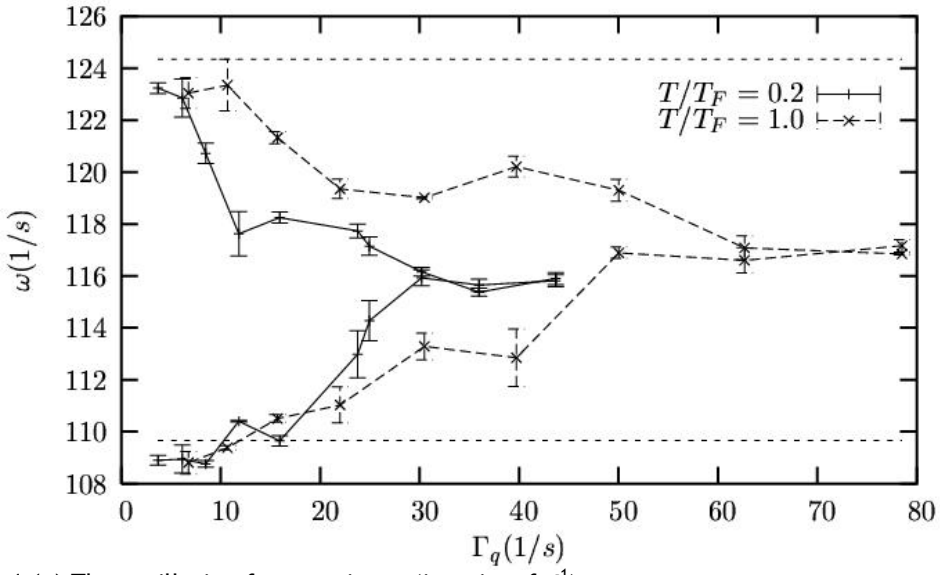

Figure 1 (a) The oscillation frequencies ω (in units of s^{-1})

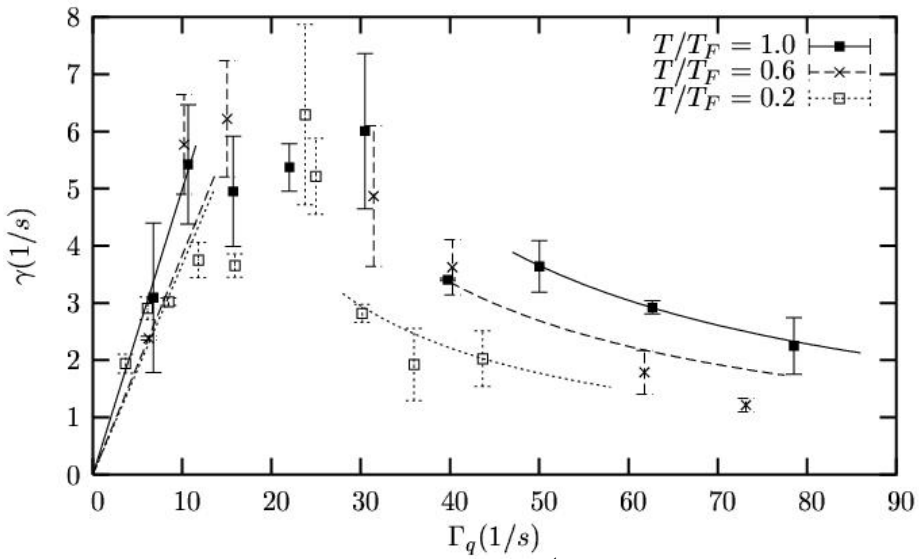

Figure 1 (b) The damping coefficient γ (in units of s^{-1}) as functions of the quantum collision rate Γ_q (in units of s^{-1}) for the two components of the gas at various temperatures. The horizontal dashed lines show the bare trap frequencies.

The main original result of our first study is to show that the locking transition shifts to lower Γ_q as temperature is decreased. This is shown in Fig. 2. This effect is a consequence of Fermi statistics: at low temperature the collisions involve particles in a narrower region around the Fermi level and a smaller number of collisions is needed to produce locking of the two species.

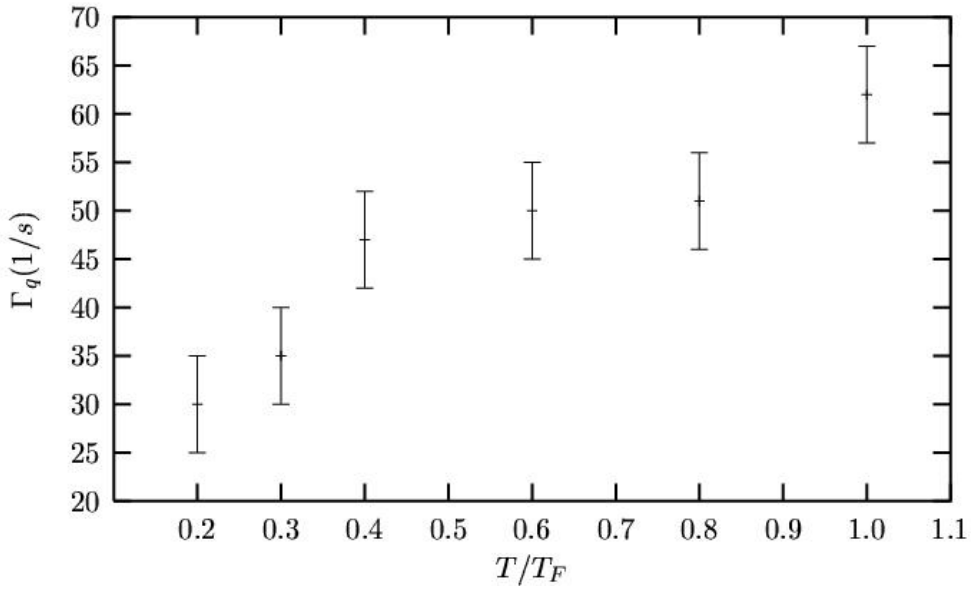

Figure 2 The collision rate Γ_q at frequency locking as a function of temperature (in units of T_F).

Efforts to develop a concurrent code, including the Pauli principle in the Lagrangian evolution to treat the collisional Fermi gas well below 0.2 T_F , are currently under way. These further studies should allow us to investigate a strategy to circumvent the Pauli blocking problem in new experiments.

Collaborations

This activity is carried out in collaboration with CNR-Istituto Applicazioni del Calcolo "Mauro Picone".

References

[1] M. H. Anderson, J. R. Ensher, M. R. Matthews, C. E. Wieman, and E. A. Cornell, Science **269**, 198 (1995); K. B. Davis, M.-O. Mewes, M. R. Andrews, N. J. van Druten, D. S. Durfee, D. M. Kurn, and W. Ketterle, Phys. Rev. Lett. **75**, 3969 (1995); C. C. Bradley, C. A. Sackett, and R. G. Hulet, *ibid* **78**, 985 (1997).

[2] S. D. Gensemer and D. S. Jin, Phys. Rev. Lett. **87**, 173201 (2001); B. De Marco and D. S. Jin, *ibid* **88**, 040405 (2002).

[3] F. Toschi, P. Vignolo, S. Succi, and M. P. Tosi, Phys. Rev. A **67**, 041605(R) (2003).

[4] T. Loftus, C. A. Regal, C. Ticknor, J. L. Bohn, and D. S. Jin, Phys. Rev. Lett. **88**, 173201 (2002).

QUANTUM TRANSPORT IN MESOSCOPIC SYSTEMS

Alessandro Cresti, Riccardo Farchioni, Giuseppe Grosso, Giuseppe Pastori Parravicini

The interest on quantum transport through mesoscopic conductors has increased enormously in the last years (see for instance Refs.[1], [2]) due to its relevance to a variety of theoretical aspects and experimental achievements. A main experimental and theoretical point has been the analysis of the nature and of the spatial distribution of the local currents in the devices, under applied external fields and under the constraints imposed by suitable geometries, both in the pure limit and in the presence of disorder. Recent experimental work by Topinka *et al*. [3], has enhanced interest on this subject by using a scanning microscope tip to obtain the spatial image of coherent currents through a quantum point contact in a two dimensional electron gas; the distribution of the local currents and conductances is then inferred from the changes of the conductance produced when the charged tip of the microscope is rastered on the sample. The evaluation of current profiles in mesoscopic systems in the presence of magnetic fields is also of major interest. Because of the entailed absence of time-reversal symmetry, persistent currents are possible also at equilibrium; in particular, currents in rings threaded by magnetic fields and related to the Aharonov-Bohm effect have been widely investigated and the interplay between persistent and transport currents in nonequilibrium situations has been considered. There are two main methods to calculate currents: the transfer matrix method within the Buttiker-Landauer formalism [4] and the Keldysh-Green's function method [5]. Even if the latter is more complex, it is preferable to the former mainly for the perspective it offers of a proper account of self-consistency and correlation effects beyond meanfield approaches, and the possibility of overcoming the low voltage limit typical of almost equilibrium conditions. In particular, the knowledge of nonequilibrium Green's functions allows one to describe the current flow through interacting sites, and to foresee the effects of impurities and geometric shape on the conductance.
In our study of charge transport in mesoscopic systems at NEST, we have provided a systematic analysis of current distribution both in the absence and in the presence of magnetic fields, and have clarified their nature in relation to the concept of time-reversal symmetry [6]. Within the Keldysh Green's function framework, we have analyzed microscopic currents along each bond of the mesoscopic system. The calculation of the nonequilibrium Green's function has been performed by means of a lattice model representation of the system. In this framework we have exploited the real-space renormalization method [7], [8] to handle the semi-infinite leads connected to the device; in this way it has become manageable to pick-up a generic cross-sectional plane of the device and evaluate horizontal and vertical currents flowing across it. The starting structure under investigation can be envisaged as composed by three regions; a finite central region and two semi-infinite perfect leads on the left and on the right side (see Fig. 1). The central region consists of an array of *N*x*M* sites, where the wavefunctions are localized. The two perfect leads include infinite degrees of freedom.

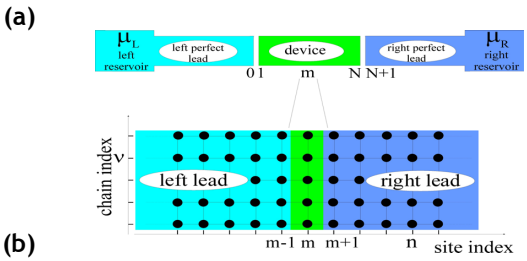

Figure 1
(a) Typical arrangement of a two-dimensional device for the analysis of current distribution;
(b) Magnification of the central device of interest (column *m*) with adjacent (redefined) leads.

We have adopted our procedure in three specific cases: **i)** for the current distribution in a Quantum Wire in the transport regime of Universal Conductance Fluctuation, **ii)** for the charge transport through Quantum Point Contacts (QPC) and **iii)** for the current distribution and conductance quantization in the integer quantum Hall regime.

i) For the study of current distribution in a random quantum wire in the transport regime of **Universal Conductance Fluctuation** we have adopted a two-dimensional quantum wire of *M*=50 infinite chains,

with nearest neighbours interactions and one orbital per site. The hopping parameters are taken all equal to $-t$, and the positive quantity $|t|$ is assumed as the unit of energy. The central device is formed by N=50 columns with M=50 sites each. The site energies are set equal to zero in the perfect leads. In the 2500 sites of the central device, the Anderson model of disorder is adopted. In the calculations the disorder strength is taken to be W=3.5t. The total conductance exhibits rather sharp fluctuations, whose "universal" magnitude is of the order of $2e^2/h$. It is seen that the total conductance of the wire, when non negligible, reaches values smaller than $2e^2/h$, indicating that no more than a single conductance channel is active. The conductance profile of the disordered quantum wire is given in Fig. 2 for the Fermi energy E_F=3.601t. The total conductance through any transversal section of the system is 0.635x $2e^2/h$. The behavior of the currents includes vortices (Fig. 2(b)), which do not contribute to the net charge transport, and regions of more regular current flow (Fig. 2(c)), where the longitudinal bond conductance remains of the order of $2e^2/h$.

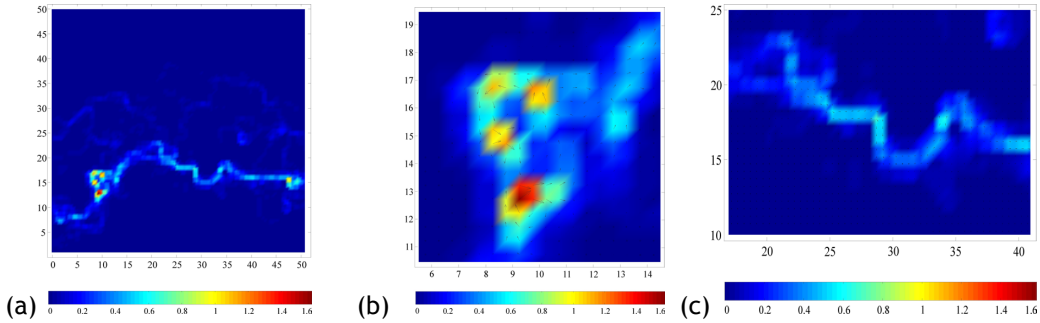

Figure 2 (a) Spatial conductance profile of a disordered quantum wire in the universal conductance fluctuation regime. **(b)** a particular of (a) to illustrate a region of current vortices. **(c)** a particular of (a) to illustrate details of the current path.

The effect of a uniform magnetic field on the disordered device is to change slightly the position of the conductance peak under investigation while increasing significantly the maximum to the value 0.828x $2e^2/h$. Correspondingly, the magnetic field completely alters the distribution of the current flow. Although the total conductance through any orthogonal section of the system is $0.828x2e^2/h$, the effect of the magnetic field is to generate regions of high conductances in the form of vortices.

ii) Charge transport through a Quantum Point Contacts (QPC) [9].

We have addressed the problem of the currents distribution through a quantum point contact device (of the form proposed by Buttiker -Fig. 3(b)-) with reference to the work of Topinka *et al*. where the difference of conductance in the presence and in the absence of a scanning probe microscope tip are measured (see Fig. 3(a)).

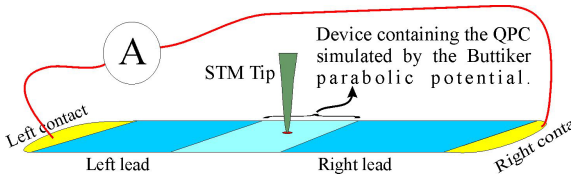

Figure 3 (a)

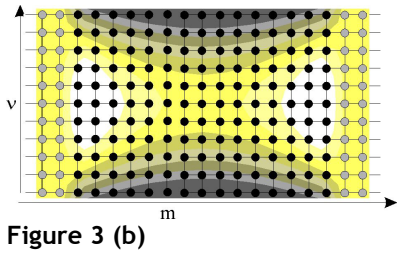

Figure 3 (b)

We have provided detailed maps of currents distribution through a QPC by means of the nonequilibrium Keldysh formalism. Then we have compared these maps with the corresponding ones obtained by the difference of conductance in the presence and in the absence of the scanning tip which is mimicked by adding the scattering potential W_{tip} to the background energy potential of the device.

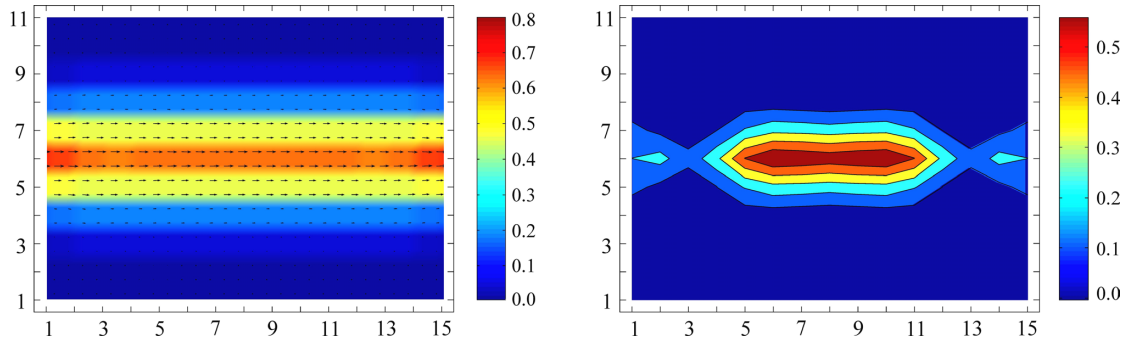

(a) **(b)**

Figure 4 (a) Map of the currents distribution obtained by the Keldysh-Green's function method in the absence of the tip; **(b)** Map of the conductance changes inferred with the "tip method".

The distribution calculated with our method is substantially homogenous in the longitudinal direction through the QPC. The distribution of currents inferred with the "tip model" is reported in Fig. 4(b) and the difference between the two results is evident. The "tip method" points out zones of different conductance of the "sample plus tip" system; the interference effects apparent in Fig. 4(b) are produced by the tip scattering potential, that modifies the currents distribution according to its position above the device and does not simply block the local current. Obviously there is nothing but a small effect of the tip potential in the regions where the current flow is small, elsewhere the map of the currents is significantly altered.

In order to stress the importance of the interference effects related to the tip, we have analyzed the current distribution after locating the tip in different places above the device. For example, if the tip is placed on the right part of the device (see Fig. 5(a)) the current keeps on flowing around the obstacle with a limited influence on the total conductance; thus, with the "tip method" we do not observe much difference in the conductance as evident from Fig. 4(b). If the tip is placed in the middle of the system (see Fig. 5(b)) the flux tends to localize near the tip and the charge flow along the longitudinal direction is depressed. Thus in this case the difference between the conductance with or without the tip is larger, as evident from Fig. 4(b).

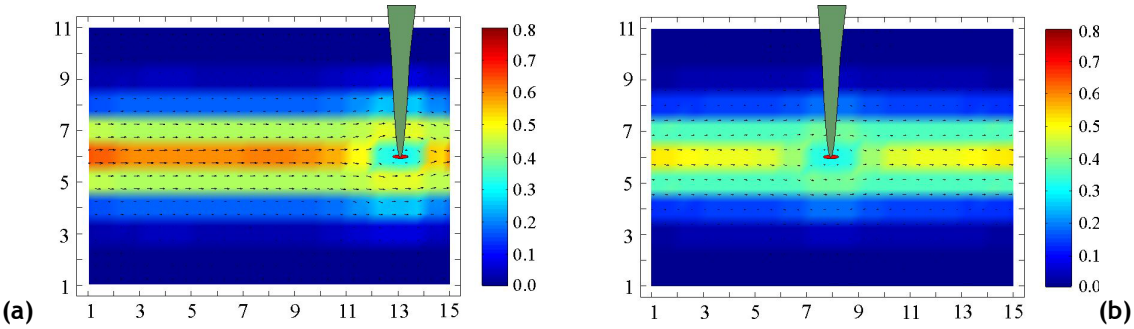

(a) **(b)**

Figure 5 Spatial currents distribution for two chosen positions of the tip **(a).** The tip is situated far from the QPC center; the current flows almost unperturbed along the device and around the obstacle. **(b)** The tip is situated at the center of the QPC; a significant depression of the conductance is shown.

In conclusion, we have seen that the maps of the spatial currents distribution inferred from the change of conductances due to the tip do not reflect in general the actual current situation, but are enriched by the peculiar coherence effects occurring in the regions where the current is present.

iii) Current distribution and conductance quantization in the integer quantum Hall regime [10].

About twenty years ago, the discovery of the integer quantum Hall effect [11] has opened a new area of research and has led to extensive investigations on the subject. The most spectacular experimental feature and theoretical challenge is the perfect quantization of the Hall conductance of a two-dimensional electron gas in integer multiples of $2e^2/h$, and its universality regardless of the type of mesoscopic device under investigation, degree of disorder, impurities, etc. The commonly accepted explanation [12] of the well defined plateaus in the quantum Hall resistance, resides in the net spatial separation of edge states supporting right and left moving carriers, so that the probability of scattering of electrons between states of reverse direction is vanishingly small.

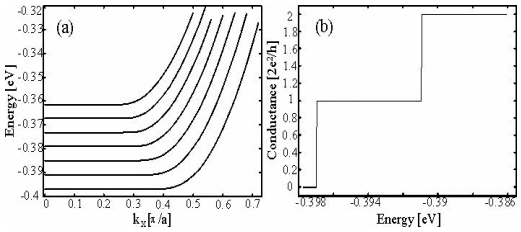

Figure 6 (a) Seven lower energy magnetic bands of the ideal wire. **(b)** Total conductance in the range [-0.398eV, -0.388eV]. Each jump in the conductance corresponds to the Fermi level intersecting a new magnetic band.

We have investigated the spatial distribution of currents in a two-dimensional electron gas threaded by a magnetic field, and have provided a vivid picture of the carriers flowing on the edges of the wire. We have found that both *persistent* currents and *transport* currents exhibit exact conductance quantization in the integer quantum Hall regime; this is true both in ideal samples without disorder and in the presence of impurities, disorder, border irregularities and other defects.

We have adopted the tight-binding framework for the description of a quantum wire and the uniform magnetic field B has been introduced through the Peierls phase factor. Additional terms, diagonal in the site representation, are later added to the Hamiltonian to represent presence of impurities or effect of disorder. From the Green's function of the Hamiltonian, eigenvalues and density of have been obtained. For a magnetic field of 5 Tesla the eigenvalues of the Hamiltonian are reported in Fig. 6(a). It can be noticed that in the central part of the Brillouin zone the magnetic bands are flat and correspond to bulk Landau levels. At the border of the Brillouin zone, the energies of the bands rise because the corresponding states approach the physical edge of the wire. It is interesting to look at the regions where currents are distributed: from Fig. 7(a) it is evident that only edge states support the current along the wire, which is composed by a transport current (Fig. 7(b)) and a persistent (top and down) current (Fig. 7(c)). The states in the bulk of the wire are inactive to charge transport. To further test the robustness of the conductance quantization versus scattering potentials, we have inserted in the wire an extended disordered region, as specified in Fig. 8. The conductance profiles exhibit deep modifications and also the formation of vortices but, as far as the flow of persistent currents occurs on spatially separated regions, each contribution to the conductance is exactly quantized in units of $2e^2/h$. In conclusion, we have shown the robustness of the exact conductance quantization both of transport currents and of spatially separated persistent currents. The occurrence of the former quantization entails negligible longitudinal potential drop when current flows across the sample; the occurrence of the latter entails exact conductance quantization when the Hall potential develops.

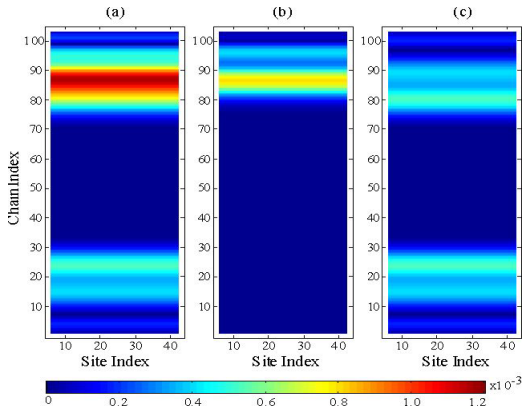

Figure 7 Spatial distribution of the total **(a)** current at the energy E=-0.396 eV, due the transport **(b)** and persistent **(c)** currents.

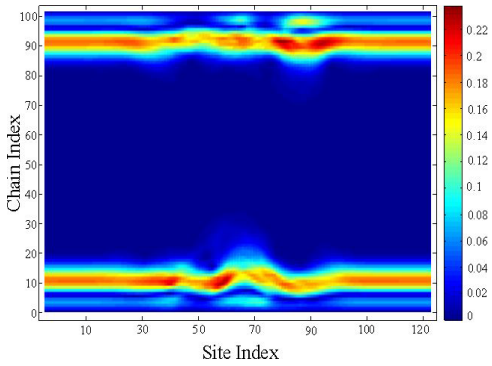

Figure 8. Conductance for random distribution of point impurities inserted in the central region of the device.

References

[1] S. Datta, *Electronic Transport in Mesoscopic Systems* (Cambridge University Press, Cambridge 1995).
[2] D. K. Ferry and S. M. Goodnick, *Transport in Nanostructures* (Cambridge University Press, Cambdridge 1997).
[3] M. A. Topinka, B. J. LeRoy, R. M. Westervelt, S. E. J. Shaw, E. J. Heller, K. D. Maranowski, and A. C. Gossard, Science **289**, 2323 (2000); M. A. Topinka, B. J. LeRoy, S. E. J. Shaw, R. M. Westervelt, R. Fleischmann, E. J. Heller, K. D. Maranowski, and A. C. Gossard, Nature **410**, 183 (2001).
[4] R. Landauer, IBM J. Res. Dev. **1**, 223 (1957); M. Buttiker, Phys. Rev. Lett. **57**, 1761 (1986).
[5] See for instance the review R. Lake, G. Klimeck, R. C. Bowen, and D. Jovanovic, J. Appl. Phys. **81**, 7845 (1997).
[6] A. Cresti, R. Farchioni, G. Grosso, and G. Pastori Parravicini, Phys. Rev. B. **68**, 075306 (2003).
[7] G. Grosso and G. Pastori Parravicini, *Solid State Physics* (London, Academic Press 2000).
[8] R. Farchioni, G. Grosso, and P. Vignolo "Recursive algorithms for Polymeric Chains" in Springer Series in Materials Science, Vol. **41**, pp. 89-125 (Berlin, Springer-Verlag 2001) and references quoted therein.
[9] A. Cresti, R. Farchioni, G. Grosso and G. Pastori Parravicini, Journal of Applied Physics **94**, 1744 (2003).
[10] A. Cresti, R. Farchioni, G. Grosso, and G. Pastori Parravicini, J. Phys.: Condens. Matter **15**, L377 (2003).
[11] K. von Klitzing, G. Dorda, and M. Pepper, Phys. Rev. Lett. **45**, 494 (1980).
[12] M. Buttiker, Phys. Rev. B **38**, 9375 (1988).

PHOTONIC CRYSTALS

Alessandra Toncelli, Francesco Cornacchia, Elisa Sani, Mauro Tonelli

This activity is devoted to the development of optical fiber crystals based on fluoride and oxide compounds: it is the natural evolution from macroscopic systems (bulk crystals) to micro-systems (fibers), and it is aimed at the development of new laser sources and at the study of frequency conversion devices. The development of single-crystal fibers offers at least two advantages with respect to bulk crystals, namely the possibility of studying new types of materials at reduced costs, and of designing high-efficiency sources of small size. The growth technique is "micro pulling-down", the fiber will have a diameter between 0.1 and 1 mm and a length up to 50 cm.

Figure 1

The furnace for the fiber growth consists in a circular central body of 250 mm diameter closed at the top and bottom with flanges. The vacuum system is composed by a primary pump and a turbo-molecular pump to obtain a vacuum value of about 10^{-7} mbar. In these experimental conditions the chamber is isolated by a gate vacuum valve and filled with high-purity Argon gas to avoid contamination of the growth powders and oxidation of the crucible. At the bottom of the chamber a bellow allows the pulling of the seed upward and downward. The heating of the crucible is obtained with a copper coil cooled by water. It is put inside the vacuum chamber by a special feedthrough and fed by a RF generator. The temperature of the crucible and the stepping-motor for pulling the seed is controlled by computer. The assembly of the all apparatus (μm-Pd furnace and red RF generator) is shown in Fig. 1.

The crucible for the micro pulling-down technique has a special structure made in two parts. The first part is cylindrical with a conical shape at the bottom. It contains the powders and it has a hole at the bottom (diameter 0.5 mm) where the crystal fiber is pulled from. The second part is cylindrical and it is used as after-heater to avoid excessive temperature gradients to the fiber during the growth. In Fig. 2 we show the whole structure. We used two different crucibles: Iridium and graphite according to the chemical conditions.

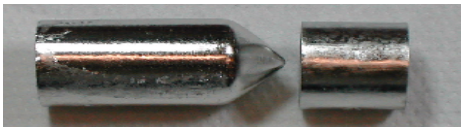

Figure 2

Thanks to this set up, we reported the growth of the first LiF crystalline fibers. We grew these fibers in the graphite crucible and in Argon atmosphere to avoid OH contamination. The presence of these radicals, even at very low concentration (~ 5-10 ppm), can compromise the optical quality of the material.

The experimental conditions are the following: crucible temperature 775°C, pulling rate 0.5 mm/min. Fiber length 130 mm, fiber diameter 500 μm, growth time about five hours.

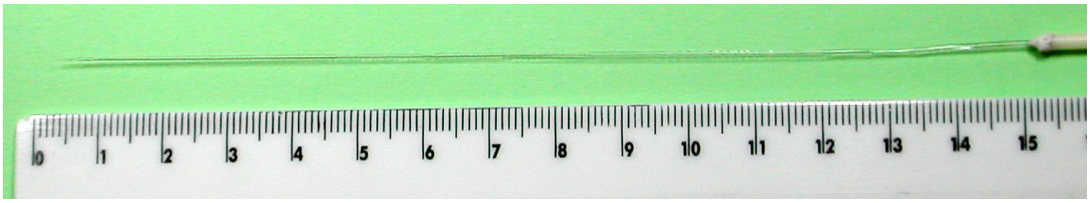

Figure 3

The crystal fiber is shown in Fig. 3. It is transparent and the fluctuation of its diameter is about 10%. We also performed a structural analysis by RX Laue technique and verified the mono-crystalline structure of the sample.

Collaborations

This activity is carried out in collaboration with Tsukuba University, Japan, Institut für Laser-Physik Hamburg, Germany, Physikalisch-Technische Bundesanstalt Braunschweig, Germany, and INFM-Parma.

References

[1] E. Osiac, E. Heumann, G. Huber, S. Kück, E. Sani, A. Toncelli, and M. Tonelli, "Orange and red upconversion laser pumped by an avalanche mechanism in Pr3+, Yb3+, BaY2F8" Appl. Phys. Lett. **82**, 3832 (2003).

[2] F. Cornacchia, L. Palatella, A. Toncelli, M. Tonelli, A. Baraldi, R. Capelletti, E. Cavalli, K. Shimamura, and T. Fukuda "Temperature dependence of impurity quenched luminescence in Tm3+: LiLuF4" J. Phys. Chem. Solids **63**, 197 (2002).

[3] A. Agnesi, S. Dell'Acqua, A. Guandalini, G. Reali, F. Cornacchia, A. Toncelli, M. Tonelli, K.Shimamura, and T. Fukuda "Optical Spectroscopy and Diode-Pumped Laser Performance" IEEE Journ. Quantum Electron. **37**, 304-313, (2001).

[4] L. Palatella, A. Di Lieto, P. Minguzzi, A. Toncelli, and M. Tonelli "Er3+doped crystals: frequency analysis of nonlinear energy transfer" J. Opt. Soc. Am. B **18**, 1711-1717 (2001).

[5] F. Cornacchia, A. Di Lieto, P. Maroni, P. Minguzzi, A. Toncelli, M. Tonelli, E. Sorokin, and I. T. Sorokina "A cw Ho, Tm: YLF laser pumped at 1.682 micron" Appl. Phys. B **73,** 191-194, (2001).

PUBLICATIONS 2003

G. De Chiara and G. M. Palma "Berry phase for a spin ½ particle in a classical fluctuating field" Phys. Rev. Lett. 91, 090404 (2003).

S. Luin, V. Pellegrini, A. Pinczuk, B.S. Dennis, L. N. Pfeiffer, and K. W. West "Observation of soft magnetorotons in bilayer quantum Hall ferromagnets" Phys. Rev. Lett. 90, 236802 (2003).

D. Dini, R. Köhler, A. Tredicucci, G. Biasiol, and L. Sorba "Microcavity polariton splitting of intersubband transitions" Phys. Rev. Lett. 90, 116401 (2003).

R. Köhler, A. Tredicucci, F. Beltram, H. E. Beere, E. H. Linfield, A. G. Davies, and D. A. Ritchie "Low-threshold quantum-cascade lasers at 3.5 THz (λ = 85 μm)" Opt. Lett. 28, 810 (2003).

S. Barbieri, J. Alton, S. S. Dhillon, H. E. Beere, M. Evans, E. H. Linfield, A. G. Davies, D. A. Ritchie, R. Köhler, A. Tredicucci, and F. Beltram "Continuous-wave operation of Terahertz quantum-cascade lasers" IEEE J. Quantum Electron. 39, 586 (2003).

R. Köhler, A. Tredicucci, F. Beltram, H. E. Beere, E. H. Linfield, A. G. Davies, D. A. Ritchie, S. S. Dhillon, and C. Sirtori "High performance continuous-wave operation of superlattice terahertz quantum cascade lasers" Appl. Phys. Lett. 82, 1518 (2003).

A. Tredicucci "TeraHertz: the new challenge for Quantum Cascade Lasers" Proceedings of 26th International Conference on Infrared and Millimeter Waves (INCMP, Toulouse, 2003).

C. Capuzzi, A. Minguzzi, and M. P. Tosi "Collective excitations of a trapped boson-fermion mixture acros demixing" Phys. Rev. A. 68, 53605 (2003).

B. Davoudi, R. Asgari, M Polini, and M. P. Tosi "Self-consistent scattering theory of the pair distribution function in charged Bose fluids" Phys. Rev. B. 67, 172503 (2003).

P. Vignolo, A. Minguzzi "Shell structure in the density profiles for noninteracting fermions in anisotropic harmonic confinement" Phys. Rev. A. 67, 53601 (2003).

R. Asgari, M. Polini, V. Carnevale, and M. P. Tosi "Vibrational excitations in the paired phases of a two-dimensional electron crystal in a perpendicular magnetic field" Physica B 336, 387 (2003).

B. Davoudi, R. Asgari, M. Polini, and M. P. Tosi "Analytic theory of ground-state properties of a three-dimensional electrongas with arbitrary spin polarization" Phys. Rev. B 68, 155112 (2003).

Z. Akdeniz, P. Vignolo, and M. P. Tosi "Collective dynamics of fermion clouds in cigar-shaped traps" Phys. Lett. A 311, 246 (2003).

N. H. March, M. P. Tosi, and A. Minguzzi "Can trimers influence the free surface density profile of liquid 4He atzero temperature ? " J. Chem. Phys. 119, 4597 (2003).

P. Capuzzi, A. Minguzzi, and M. P. Tosi "Collective excitations in trapped boson-fermion mixtures: From demixing to collapse" Phys. Rev. A 68, 033605 (2003).

A. Minguzzi, N. H. March, and M. P. Tosi "Superfluidity with and without a condensate in interacting Bose fluids" -, Phys. Chem. Liquids 41, 323 (2003).

A. Cresti, R. Farchioni, G. Grosso, and G. Pastori Parravicini "Investigation of spatial currents imaging in mesoscopic systems" Journal of Applied Physics 94, 1744 (2003).

A. Cresti, R. Farchioni, G. Grosso, and G. Pastori Parravicini "Current distribution and conductance quantization in the integer quantum Hall regime" J. Phys.: Condens. Matter 15, L377 (2003).

A. Cresti, R. Farchioni, G. Grosso, and G. Pastori Parravicini "Keldysh-Green's function formalism for currents profiles in mesoscopic systems", Phys. Rev. B 68, 075306 (2003).

V. Tozzini, A. R. Bizzarri, V. Pellegrini, R. Nifosì, P. Giannozzi, A. Iuliano, S. Cannistraro, and F. Beltram "The low frequency vibrational modes of Green Fluorescent Proteins" Chem. Phys. 287/1-2, 33-42 (2003).

R. Nifosì and V. Tozzini "Molecular dynamics simulations of enhanced green fluorescent proteins: Effects of F64L, S65T and T203Y mutations on the ground-state proton equilibria" Proteins 51, 378 (2003).

R. Nifosì, A. Ferrari, C. Arcangeli, V. Tozzini, V. Pellegrini, and F. Beltram "Photoreversible dark state in a tristable Green Fluorescent Protein variant" J. Phys. Chem B 107, 1679-1684 (2003).

R. Asgari, B. Davoudi, M. Polini, and M. P. Tosi "Pair densities at contact in the quantum electron gas" Solid State Commun. 125, 139 (2003).

L. Faoro, J. Siewert, and R. Fazio "Non-Abelian phases, pumping, and quantum computation with Josephson junctions" Phys. Rev. Lett. 90, 028301 (2003).

G. Falci, R. Fazio, and G. M. Palma "Quantum gates and Berry phases in Josephson nanostructures" Fortschritte der Physik 51, 442 (2003).

E. Osiac, E. Humann, G. Huber, S. Kuck, E. Sani, A. Toncelli, and M. Tonelli "Orange and red upconversion laser pumped by an avalanche mechanism in Pr3+, Yb3+, BaY2F8" Appl. Phys. Lett, 82, 3832 (2003).

F. Giazotto, F. Taddei, R. Fazio, and F. Beltram "Ferromagnetic resonant tunneling diodes as spin polarimeters and polarizers" Appl. Phys. Lett. 82, 2449 (2003).

F. Toschi, P. Vignolo, S. Succi, and M. P. Tosi "Dynamics of trapped two-component Fermi gas,: Temperature dependence of the transition from collisionless to collisional regime" Phys. Rev. A 67, 41605 (2003).

P. Vignolo, Z. Akdeniz, and M. P. Tosi "The transmittivity of a Bose-Einstein condensate on a lattice: interference from period doubling and the effect of disorder" J. Phys. B 36, 4535 (2003).

S. Roddaro, V. Pellegrini, F. Beltram. G. Biasiol, L. Sorba, R. Raimondi, and G. Vignale "Nonlinear quasiparticle tunneling between fractional quantum Hall edges" Phys. Rev. Lett. 90, 046805 (2003).

M. Cecchini, V. Piazza, F. Beltram, M. Lazzarino, M. B. Ward, A. J. Schields, H. E. Beere, and D. A. Richie "High-performance planar light emitting diodes" Appl. Phys. Lett. 82, 636 (2003).

M-S Choi, F. Plastina, and R. Fazio "Charge and current fluctuations in a superconducting single electron transistor near a Cooper pair resonance" Phys. Rev. B 67, 45105 (2003).

A. Marcello, A. Ferrari, V. Pellegrini, G. Pegoraro, M. Lusic, F. Beltram, and M. Giacca "Recruitment of human Cyclin T1 to nuclear bodies through direct interaction with the PML protein", EMBO Journal 22, 2156 (2003).

E. Tasciotti, M. Zoppe, and M. Giacca "Transcellular transfer of active HSV-1 thymidine kinase mediated by an 11-amino-acid peptide from HIV-1 Tat" Cancer Gene Ther. 10, 64 (2003).

V. Piazza, V. Pellegrini, F. Beltram, and W. Wegscheider "Metastable phase in the quantum Hall ferromagnet" Solid State Communications 127, 163 (2003).

G. Falci, R. Fazio, and A. Mastellone "Interplay between pairing and exchange in small metallic dots" Phys. Rev. B 67, 132501 (2003).

A. Braggio, R. Fazio, and M. Sassetti "Shot noise of a quantum dot with non-Fermi-liquid correlations" Phys. Rev. B 67, 233308 (2003).

L. Faoro, J. Siewert, and R. Fazio "Non-Abelian phases, charge pumping, and holonomic computation with Josephson junctions", Phys. Rev. Lett. 90, 028301 (2003).

V. Cataudella and R. Fazio "Glassy dynamics of Josephon arrays on a dice lattice" Europhys. Lett. 61, 341 (2003).

G. Franzese, R. Raimondi, and R. Fazio "Parity-dependent Kondo effect in ultrasmall metallic grains" Europhys. Lett. 62, 264 (2003).

G. Biasiol, L. Sorba, D. Dini, A. Tredicucci, and F. Beltram "Electron-phonon strong coupling in intersubband resonator", in Compound Semiconductors 2002, Ed. by M. Ilegems, G. Weimann and J. Wagner, Institute of Physics Conference Series **174** (IOP Publishing Bristol and Philadelphia 2003), p. 389.

A. Ferrari, V. Pellegrini, C. Arcangeli, A. Fittipaldi, M. Giaccca, and F. Beltram "Caveolae-mediated internalization of extracellular HIV-1 Tat fusion proteins visualized in real time", Mol. Ther. 8, 284 (2003).

V. Tozzini, V. Pellegrini, and F. Beltram "Green Fluorescent Proteins and their applications to cell biology and bioelectronics", in Handbook of organic photochemistry and photobiology, Chapter 139, W. M. Horsphool and F. Lenci, Eds., CRC Press/Lewis Publisher (2003).

A. Fittipaldi, A. Ferrari, M. Zoppé, C. Arcangeli, V. Pellegrini, F. Beltram, and M. Giacca "Cell membrane lipid rafts mediate caveolar endocytosis of HIV-1 Tat fusion proteins". J Biol Chem. 278, 34141 (2003).

- *in press* -

R. Asgari, M. Polini, B. Davoudi, and M. P. Tosi "Correlation energy of a two-dimensional electron gas from static and dynamic exchange-correlation kernels" Phys. Rev. B. *in press* (2003).

D. C. Marinescu and M. P. Tosi "Spin transresistivity - a probe of the opposite spin correlations in anelectron system" Solid State Commun. *in press* (2004).

M. Polini, R. Fazio, A. H. MacDonald, J. Sinova, and M. P. Tosi "Frustration of a Bose gas inside an optical lattice" Laser Phys. *in press* (2004).

P. Capuzzi, A. Minguzzi, and M. P. Tosi "Dynamic versus thermodynamic signatures of quantum demixing under confinement" Laser Phys. *in press* (2004).

G. Falci, A. Fubini, A. Mastellone, and R. Fazio "Universal features of pairing and exchange in ultra-small superconducting grains" Physica B *in press* (2003).

PUBLICATIONS 2002

R. Köhler, A. Tredicucci, F. Beltram, H. E. Beere, E. H. Linfield, A. G. Davies, D. A. Ritchie, R. Iotti, and F. Rossi "THz semiconductor-heterostructure laser" Nature 417, 156 (2002).

R. Köhler, A. Tredicucci, F. Beltram, H. E. Beere, E. H. Linfield, A. G. Davies, and D. A. Ritchie "High-intensity interminiband terahertz emission from chirped superlattices" Appl. Phys. Lett. 80, 1867 (2002).

R. Köhler, A. Tredicucci, F. Beltram, H. E. Beere, E. H. Linfield, A. G. Davies, D. A. Ritchie, R. Iotti, and F. Rossi "THz semiconductor heterostructure laser" Physics of semiconductors 2002 - Proceedings of the 26th International Conference.

F. Giazotto, F. Taddei, R. Fazio, and F. Beltram "Ultraefficient cooling in ferromagnet-superconductor microrefrigerators" Appl. Phys. Lett. 80, 3784 (2002).

S. Roddaro, V. Piazza, F. Beltram, W. Wegscheider, C. T. Liang, and M. Pepper “Magnetotransport in variable-coupling one-dimensional ballistic constrictions” J. of Appl. Phys. 92, 5304 (2002).

R. Köhler, A. Tredicucci, F. Beltram, H. E. Beere, E. H. Linfield, A. G. Davies, D. A. Ritchie, R. Iotti, and F. Rossi "Terahertz quantum cascade lasers" Radiation-matter interaction in confined systems (Società Italiana di Fisica, Bologna, 2002).

B. Davoudi, M. Polini, G. Sica, and M. P. Tosi "Effective interactions between parallel-spin electrons in two-dimensional jellium approaching the magnetic phase transition" Solid State Communications. 12, 295-299 (2002).

B. Davoudi, A. Minguzzi, and M. P. Tosi "Hartree-Fock-Bogoliubov theory of a charged Bose gas at finite temperature" Phys. Rev. B 6514, 4507 (2002).

M. Polini, K. Moulopoulos, B. Davoudi, and M. P. Tosi "Unpaired and spin-singlet paired states of a two-dimensional electron gas in a perpendicular magnetic field" Phys. Rev. B 65, 165306 (2002).

B. Davoudi and M. P. Tosi "Spin polarization in a two-dimensional electron gas" Physica B. 322, 124-132 (2002).

A. Minguzzi, B. Davoudi, and M. P. Tosi "Single-particle density matrix and superfluidity in the two-dimensional Bose Coulomb fluid" Phys. Rev. B 66, 054538 (2002).

B. Davoudi, M. Polini, R. Asgari, and M. P. Tosi "Self-consistent Overhauser model for the pair distribution function of an electron gas in dimensionalities D=3 and D=2" Phys. Rev. B 66, 075110 (2002).

B. Davoudi, M. Polini, and M. P. Tosi "Spin-density functional approach to thermodynamic and structural consistence in the charge and spin response of an electron gas" Solid State Communications. 124, 335 (2002).

F. Capurro, R. Asgari, B. Davoudi, M. Polini, and M. P. Tosi "Pair densities in a two-dimensional electron gas (jellium) at strong coupling from scattering theory with Kukkonen-Overhauser effective interactions" Zeitschrift fur Naturforschung Section A-A Journal of Physical Sciences 57, 237 (2002).

Z. Akdeniz, P. Vignolo, A. Minguzzi and M. P. Tosi "Phase separation in a boson-fermion mixture of Lithium atoms" J. Phys. B 35, L105 (2002).

Z. Akdeniz, A. Minguzzi, P. Vignolo, and M. P. Tosi "Demixing in mesoscopic boson-fermion clouds inside cylindrical harmonic traps: quantum phase diagram and the role of temperature" Phys. Rev. A 66, 013620 (2002).

A. Minguzzi, P. Vignolo, and M. P. Tosi "High-momentum tails in the Tonks gas under harmonic confinement" Phys. Lett. A 294, 222 (2002).

P. Vignolo, A. Minguzzi, and M. P. Tosi "Degenerate gases under harmonic confinement in one dimension: rigorous results in the impenetrable-bosons/spin-polarized-fermions limit" Int. J. Mod. Phys. B 16, 2161 (2002).

A. Osterloh. L. Amico, G. Falci, and R. Fazio "Scaling of Entanglement close to a Quantum Phase Transitions" Nature 416, 608 (2002).

E. Paladino, L. Faoro, G. Falci, and R. Fazio "Decoherence and 1/f noise in Josephson qubits" Phys. Rev. Lett. 88, 228304 (2002).

F. Taddei and R. Fazio "Counting statistics for entangled electrons" Phys. Rev. B 65, 075317 (2002).

F. Taddei and R. Fazio "Positive cross-correlations induced by ferromagnetic contacts" Phys. Rev. B 65, 134522 (2002) on-line journal.

J. Siewert, L. Faoro, and R. Fazio "Holonomic quantum computation with Josephson networks" Phys. Stat. Sol. 233, 490 (2002).

F. Plastina, R. Fazio, and G. M. Palma "Entanglement detection in Josephson nanocircuits" J. Mod. Optics 49, 1389 (2002) on-line journal.

J. Siewert and R. Fazio "Implementation of the Deusch-Jozsa algorithm with Josephson charge qubits" J. Mod. Optics 49, 1245 (2002) on-line journal.

E. Paladino, L. Faoro, G. Falci, and R. Fazio "Decoherence due to background charges in Josephson devices" Proc. of the MS2002, H. Takayanagi Ed.

F. Giazotto, F. Taddei, R. Fazio, and F. Beltram "Ultra-efficient Cooling in Ferromagnet-Superconductor Microrefrigerators" Appl. Phys. Lett. 80, 3784 (2002).

G. Falci, A. Fubini, and A. Mastellone "Mesoscopic fluctuations in superconducting dots at finite temperatures" Phys. Rev. B 65, 140507 (2002).

S. Caracciolo, M. Papinutto, and A. Pelissetto "Dynamics critical behavior of an extended reptation dynamics for self-avoiding walks" Phys. Rev. E 65, 31106 (2002).

J.-M. Jancu, F. Bassani, F. Della Sala, and R. Scholz "Transferable tight-binding parametrization for the group III nitrides" Appl. Phys. Lett. 81, 4838 (2002).

C. Cavazzoni, R. Colle, R. Farchioni, and G. Grosso "Car-Parrinello molecular dynamics study of electronic and structural properties of neutral polyanilines" Phys. Rev. B 66, 165110 (2002).

M. Lazzarino, S. Heun, B. Ressel, K. C. Prince, P. Pingue, and C. Ascoli "Atomic force microscope anodic oxidation studied by spectroscopic microscopy" Appl. Phys. Lett. 81, 2842 (2002).

F. Cornacchia, L. Palatella, A. Toncelli, M. Tonelli, A. Baraldi, R. Capelletti, E. Cavalli, K. Shimamura, and T. Fukuda "Temperature dependence of impurity quenched luminescence in Tm3+: LiLuF4" J. Phys. Chem. Solids 63, 197 (2002).

PUBLICATIONS 2001

V. Tozzini and R. Nifosì "Ab Initio Molecular Dynamics of the GFP Chromophore: An Insight into the Photoinduced Dynamics of Green Fluorescent Proteins" J. Phys. Chem. B 105, 5797 (2001).

R. A. G. Cinelli, V. Pellegrini, A. Ferrari, P. Faraci, R. Nifosì, M. Tyagi, M. Giacca, and F. Beltram "Green fluorescent proteins as optically controllable elements in bioelectronics" Appl. Phys. Lett. 79, 3353 (2001).

V. Tozzini, F. Buda, and A. Fasolino "Fullerene-like III-V clusters: a Density Functional Theory Prediction" J. Phys. Chem. B. 105 12477-12480 (2001).

R. A. G. Cinelli, V. Tozzini, V. Pellegrini, F. Beltram, G. Cerullo, M. Zavelani-Rossi, S. De Silvestri, M. Tyagi, and M. Giacca "The coherent dynamics of photoexcited green fluorescent proteins" Phys. Rev. Lett. 86, 3439 (2001).

R. Köhler, R. C. Iotti, A. Tredicucci, and F. Rossi "Design and simulation of THz quantum cascade lasers" Appl. Phys. Lett. 79, 3920 (2001).

M.-S. Choi, R. Fazio, J. Siewert, and C. Bruder "Coherent Oscillations in a Cooper-Pair Box" Europhys. Lett. 53, 251 (2001).

G. Falci, R. Fazio. G.M. Palma, J. Siewert, and V. Vedral "Geometric Quantum Computation with Josephson Qubits" Physica C 352, 110 (2001).

F. Plastina, R. Fazio, and G. M. Palma "Macroscopic entanglement in Josephson nanocircuits" Phys. Rev. B 64, 113306 (2001).

L. Amico, G. Falci, and R. Fazio "The BCS model and the off shell Bethe ansatz for vertex" J. Phys. A 34, 6425 (2001).

M.-S. Choi, F. Plastina, and R. Fazio "Shot noise for resonant Cooper pair tunneling" Phys. Rev. Lett. 87, 116601 (2001).

D. Boese and R. Fazio "Thermoelectric effects in Kondo correlated quantum dots" Europhys. Lett. 56, 576 (2001).

J. Siewert and R. Fazio "Quantum algorithms for Josephson networks" Phys. Rev. Lett. 87, 257905 (2001).

R. Fazio, Y. Makhlin, and G. Schon, introductory notes in "Quantum Computation and Quantum Information Theory", reprinted volume with introductory notes Edited by. C. Macchiavello, G. M. Palma and A. Zeilinger, World Scientific, Singapore (2001).

"The BCS model and six vertex models" L. Amico, G. Falci and R. Fazio, Proc. of the International School of Theoretical Physics, Symmetry an d Structural Properties of Condensed Matter, T. Lulek, B. Lulek and A. Wal Eds., World Scientific Singapore (2001).

S. Luin, V. Pellegrini, F. Beltram, X. Marcadet, and C. Sirtori "Interplay between disorder and intersubband collective excitations in the two-dimensional electron gas" Phys. Rev. B 64, 041306(R) (2001).

R. A. G. Cinelli, A. Ferrari, V. Pellegrini, A. Signorelli, M. Tyagi, M. Giacca, and F. Beltram "Engineering single-molecule fluorescence dynamics for advanced biomolecular applications" Aust. J. Chem. 54, 107 (2001).

V. Pellegrini and A. Pinczuk "Excitonic spin instabilities and continuous phase transitions in quantum Hall magnets", Solid State Commun. 119, 301 (2001).

A. Marcello, R. Cinelli, A. Ferrari, G. Signorelli, M. Tyagi, V. Pellegrini, F. Beltram, and M. Giacca "Visualization of in-vivo direct interaction between HIV-1 Tat and human cyclin T1 in specific cellular compartments by fluorescence resonant energy transfer" J. of Biological Chemistry 276, 39220 (2001).

A. Agnesi, S. Dell'Acqua, A. Guandalini, G. Reali, F. Cornacchia, A. Toncelli, M. Tonelli, K. Shimamura, and T. Fukuda "Optical Spectroscopy and Diode-Pumped Laser Performance" IEEE Journ. Quantum Electron. 37, 304 (2001).

L. Palatella, A. Di Lieto, P. Minguzzi, A. Toncelli, and M. Tonelli "Er3+doped crystals: frequency analysis of nonlinear energy transfer" J. Opt. Soc. Am. B 18, 1711 (2001).

F. Cornacchia, A. Di Lieto, P. Maroni, P. Minguzzi, A. Toncelli, M. Tonelli, E. Sorokin, and I. T. Sorokina "A cw Ho, Tm: YLF laser pumped at 1.682 micron" Appl. Phys. B 73, 191 (2001).

B. Davoudi, M. Polini, G. F. Giuliani, and M. P. Tosi "Analytical expression for the spin-spin local-field factor and the spin-asymmetric exchange-correlation kernel of a twodimensional electron gas" Phys. Rev. B 64, 233110 (2001).

B. Davoudi, M. Polini, G. F. Giuliani, and M. P. Tosi "Analytical expression for the charge-charge local-field factor and the exchange and correlation kernel of a two dimensional electron gas" Phys. Rev. B 64, 153101 (2001).

P. Vignolo and A. Minguzzi "One-dimensional non-interacting fermions in harmonic confinement: equilibrium and dynamical properties" J. Phys. B 34, 4653 (2001).

F. Giazotto, P. Pingue, F. Beltram, M. Lazzarino, D. Orani, S. Rubini, and A. Franciosi "Resonant transport in Nb/GaAs/AlGaAs heterostructures: Realization of the de Gennes-Saint-James model" Phys. Rev. Lett. 87, 216808 (2001).

D. Boese and R. Fazio "Thermoelectric effects in Kondo correlated quantum dots" Europhys. Lett. 56, 576 (2001).

OUTREACH, TRAINING AND EDUCATION

OUTREACH

In line with the programme, NEST established a call for proposal scheme for research activities taking advantage of the Centre facilities. During the first two years the following projects were selected and funded:

Nanodispositivi superconduttori per l'elettronica, proponent: Prof. Francesco Tafuri (INFM-Naples)

Synthesis of fluorescent probes and their use in multicolor imaging of Tat protein and trafficking in live cells, proponent: Dr. Anna Iuliano (CNR-Pisa)

Mechanisms of entry into live cells of T11-conjugated macromolecules, proponent: Dr. Monica Zoppè (CNR-Pisa)

Signature of correlations and spin in low dimensional systems, proponent: Prof. Maura Sassetti (INFM-Genova).

TRAINING

An additional activity was the call for applicants for a NEST Molecular biophysics School. Fellows attended two training periods at NEST and the APS workshop "Opportunities for Physicists in Biology - Topical Conference" in Boston. Participants were from 6 different INFM research units throughout Italy.

NEST cosponsored several Schools, Workshops and Conferences, among these:

QWIP2002, Castello di Pavone, Torino 2002

Quantum Phases at the nanoscale, Ettore Majorana Centre, Erice 2002

Entanglement at the nanoscale, ICTP, Trieste 2002

New trends in mesoscopic physics, Ettore Majorana Centre, Erice 2002

Advances in quantum information processing: from theory to experiments, Ettore Majorana Centre, Erice 2003

New Frontiers in NanoBiotechnology: monitoring protein function with single-protein resolution, ICTP, Trieste 2003

EDUCATION

Under direct NEST funding PhD fellowship were offered at Scuola Normale Superiore in Condensed Matter Physics and Molecular Biophysics (five fellowships so far). NEST attracted additional funding for PhD fellowships from Pirelli Labs and Fondazione Tronchetti Provera (three fellowships so far). All the fellows are carrying out their research work (theoretical or experimental) at NEST under the supervision of NEST scientists. The actual number of trainees is of course much larger (see page 4) and is made possible by the fact that NEST is located within and is fully part of academic institutions like the Scuola Normale Superiore and the University of Pisa. A total of 56 graduate and undergraduate students have carried out their research work at NEST in these two years underlining the impact of the center also from this point of view.

INDEX